THE PENNSYLVANIA STATE UNIVERSITY
SCHREYER HONORS COLLEGE

DEPARTMENT OF BIOMEDICAL ENGINEERING

A COMPARATIVE STUDY OF THE ANATOMY AND FUNCTIONAL MORPHOLOGY OF THE MAMMALIAN NASAL CAVITY

ANDREW P. QUIGLEY
SPRING 2015

A thesis
submitted in partial fulfillment
of the requirements
for a baccalaureate degree
in Bioengineering
with honors in Biomedical Engineering

Reviewed and approved* by the following:

Brent A. Craven
Adjunct Professor of Mechanical Engineering
Thesis Supervisor

Michael Krane
Research Associate, Applied Research Laboratory
Assistant Professor of Bioengineering
Thesis Co-Supervisor

Sheereen Majd
Assistant Professor of Bioengineering
Honors Adviser

* Signatures are on file in the Schreyer Honors College.

Abstract

The mammalian nasal cavity is an intricate anatomical structure with a wide variety of shapes, sizes, and functional roles. The elaborate nasal passages assist in presenting a convoluted, serpentine route for airflow during inhalation. As inspired air travels through the airway, a large surface area serves multiple functions such as respiratory air conditioning, filtering of contaminants, olfaction, and conservation of heat and water. Until recently, the anatomy and functional morphology of the mammalian nasal cavity were not well known. However, recent technological advances are leading to a better understanding of mammalian nasal form and function. Of the previous anatomical and morphological studies of the mammalian nasal cavity, none have included a quantitative comparative study of different species. Despite general parallels in nasal anatomy amongst most mammalian species, significant structural differences do exist. Here, we present a qualitative and quantitative comparative study of nasal anatomy and functional morphology across three orders of the class Mammalia (Carnivora, Rodentia, Ungulata). Species in this study include the house mouse (*Mus musculus*), eastern gray squirrel (*Sciurus carolinensis*), sea otter (*Enhydra lutris*), bobcat (*Lynx rufus*), coyote (*Canis latrans*), domestic dog (*Canis familiaris*), and white-tailed deer (*Odocoileus virginianus*). We present airway cross-sections, three-dimensional anatomical reconstructions of the nasal passages, and a comparative morphometric analysis that quantitatively describes airway size and shape in each specimen. Finally, the implications of these data regarding respiratory and olfactory function are considered.

Table of Contents

List of Figures

List of Tables

List of Symbols and Abbreviations

A_c	Cross-sectional area
A_s	Cumulative surface area
D_h	Hydraulic diameter
f	Sniff frequency
P	Perimeter
Re	Reynolds number
V	Cumulative internal volume
V_{ave}	Cross-sectional average velocity
Wo	Womersley number
z	Axial location
ν	Kinematic viscosity of air

Acknowledgements

First and foremost, I would like to thank my thesis adviser, Dr. Brent Craven, for the opportunities he has provided for me and for teaching me how to grow as a person, a student, and a researcher as he has guided me every step of the way. The additional insight and direction from Dr. Michael Krane, my thesis co-adviser, is very much appreciated as he stepped in to support me at ARL during the final completion of this project. I would also like to thank Thomas Neuberger for acquiring the MRI data and for technical support in processing the data. To Allison Ranslow, Joe Richter, Chris Rumple, and Alex Rygg, thank you for your support throughout the extensive segmentation process and helping me establish the foundation of this work. To Kenny Aycock, thank you for your endless technical assistance and use of your computer when mine seemed to fail. Finally, I am extremely thankful for my parents, Judy and Steve, and the rest of my family for their endless support and love throughout this entire process.

Chapter 1

Introduction

The mammalian nasal cavity is an intricate anatomical structure with a wide variety of shapes, sizes, and functional roles. The elaborate network of nasal turbinals provides a large surface area and a convoluted, serpentine route for airflow. As inspired air travels through the nasal airway, the large surface area serves multiple functions that include chemical sensing (olfaction), filtering of inspired contaminants, respiratory air conditioning, and conservation of heat and water through counter-current heat exchange (Schmidt-Nielsen et al., 1970). Until recently, the anatomy and functional morphology of the mammalian nasal cavity were not well characterized. However, recent advances in medical imaging and anatomical reconstruction techniques have permitted the non-invasive examination of the mammalian nasal fossa in unprecedented detail (e.g., Van Valkenburgh et al., 2004; Craven et al., 2007; Van Valkenburgh et al., 2011; Coppola et al., 2014; Ranslow et al., 2014; Van Valkenburgh et al., 2014a).

The "fundamental configuration" of the nasal cavity (Figure 1) remains relatively consistent in most mammals (Moore, 1981). The nasal cavity includes two bilaterally symmetric airways, separated by the nasal septum, which lead from the nares to the nasopharynx. Each nasal airway comprises three primary anatomical regions: nasal vestibule, respiratory, and olfactory. As the most rostral portion of the nasal cavity, the nasal vestibule is primarily responsible for filtration and conveying inspired air to the respiratory region. Due to a lack of appreciable vasculature, very little respiratory air conditioning occurs in the nasal vestibule,

which is lined with squamous epithelium (Craven et al., 2007; Harkema et al., 2006; Negus, 1958; Reznik, 1990).

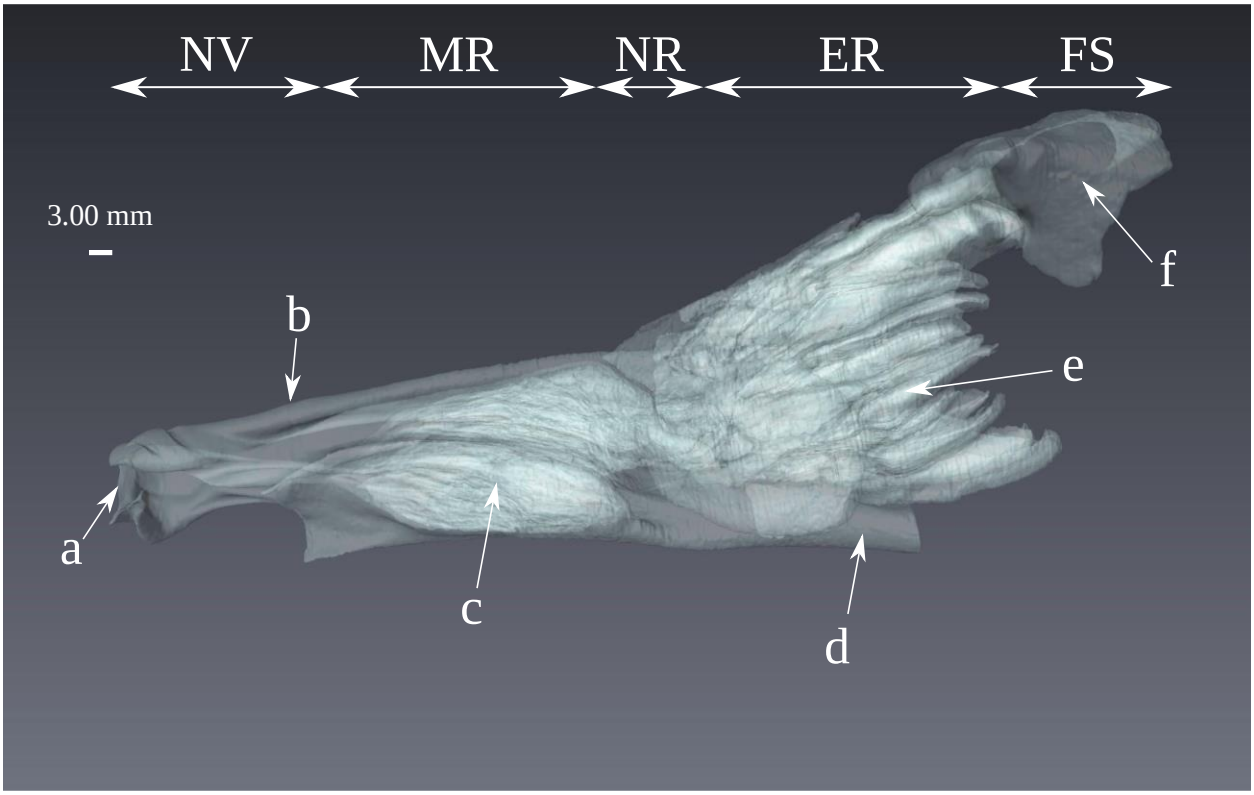

Figure 1: Sagittal representation of the mammalian nasal airway (coyote shown here). NV, nasal vestibule; MR, maxilloturbinal region; NR, nasomaxillary region; ER, ethmoidal region; FS, frontal sinus region; a, naris; b, dorsal meatus; c, maxilloturbinal; d, nasopharynx; e, ethmoturbinals; f, frontal sinus.

Continuing caudally, airflow courses through the respiratory region of the nasal cavity, where nasal conchae, or turbinals, extend from the lateral walls. Specifically, the maxilloturbinal (ventral nasal concha) and nasoturbinal (dorsal nasal concha) ramify within the respiratory region, creating a convoluted airflow path and increasing the surface area for heat and moisture exchange (Harkema et al., 2006; Moore, 1981). The walls of the respiratory region are primarily lined with respiratory epithelium (Harkema et al., 2006; Moore, 1981). Additionally, a swell body is found on either side of the nasal septum, in the ventral aspect of the respiratory region of many mammals, which is thought to regulate respiratory airflow via constriction or dilation of

the underlying vasculature (Craven et al., 2007; Negus, 1958; Reznik, 1990). That is, when the swell body is engorged it extends into the lumen and blocks much of the ventral meatus, thereby forcing airflow over the convoluted maxilloturbinal. Conversely, contraction of the swell body provides airflow with a less obstructed route through the respiratory region via the ventral meatus.

Caudal to the respiratory region is the olfactory region, where ethmoturbinals (ethmoidal conchae) that are lined with olfactory epithelium extend from the cribriform plate. In most species, the ethmoturbinals have a scroll-like morphology that provides a large surface area for odorant deposition. The ethmoturbinals can be further subdivided into ecto- and endoturbinals, depending upon the location along the mediolateral axis, where ectoturbinals comprise the lateral row and endoturbinals comprise the medial row (Moore, 1981; Negus, 1958; Van Valkenburgh et al., 2014b).

Despite general parallels in nasal anatomy among most mammalian species, some organizational and structural differences do exist. Turbinal complexity tends to vary depending on the lifestyle and functional needs of the species (e.g., see Van Valkenburgh et al., 2011), with the most complex turbinals typically found in ungulates and carnivores (Negus, 1958; Van Valkenburgh et al., 2014b). Such dramatic variation in complexity is due to the morphological differences associated with the four characteristic types of turbinals found in mammals, which, in increasing order of complexity, include: single-scroll, double-scroll, folded, and branching (Negus, 1956, 1958; Craven et al., 2007; Van Valkenburgh et al., 2014b; Richter et al., in preparation). In the respiratory region, convoluted turbinals provide a large surface area for heat and moisture exchange, and in the olfactory region complex ethmoturbinals likewise present a large surface area to the airflow for increasing odorant deposition.

The second characteristic of the nose that varies among mammals is the morphology of the olfactory region. In keen-scented (macrosmatic) animals (e.g., rodents, carnivores, ungulates), the olfactory region is relegated to a posterosuperior cul-de-sac known as the "olfactory recess," whereas feeble-scented species (e.g., humans) do not possess an olfactory recess (Craven et al., 2010; Eiting et al., 2014; Moore, 1981; Ranslow et al., 2014; Richter et al., in preparation; Van Valkenburgh et al., 2014b). In macrosmats, the olfactory recess is separated from the respiratory region by a bony plate known as the *lamina transversa* (Craven et al., 2010; Eiting et al., 2014; Evans, 1993; Moore, 1981). Also, in keen-scented species the dorsal meatus directly connects the olfactory recess to the nasal vestibule, which provides a pathway for airflow to bypass the complex respiratory region during inspiration (Craven et al., 2007; Craven et al., 2010; Lawson et al., 2012; Ranslow et al., 2014). Recent computational simulations of nasal airflow have shown the development of unique nasal airflow patterns in the macrosmatic nasal cavity that are thought to partially explain olfactory acuity in these species (Craven et al., 2010; Eiting et al., 2014). Specifically, the gross morphology of the macrosmatic nasal cavity facilitates unidirectional airflow in the olfactory region at low flow speeds, which increases odorant residence time and creates optimal conditions for chromatographic separation of odorants along the olfactory epithelium (Craven et al., 2010; Eiting et al., 2014; Lawson et al., 2012; Van Valkenburgh et al., 2014b).

To date, nasal anatomy and morphology have been investigated in a wide range of species in different mammalian orders, including Carnivora, Rodentia, and Ungulata. Specifically within the order Carnivora, where morphology tends to present a more complex structure, nasal form and function have been studied extensively. As Van Valkenburgh et al. (2014b) notes, "some of the first qualitative functional comparisons" investigating respiration

compared countercurrent heat exchange and nasal mucosa of elephant seals and phocid seals with terrestrial counterparts (Folkow et al., 1988; Huntley et al., 1984). Further studies used MRI and micro-CT data to confirm a branching maxilloturbinal structure and two distinct airflow pathways for respiration and olfaction in the domestic dog (Craven et al., 2007; Craven et al., 2010). MRI data was also used to develop a reference for normal nasal anatomy in the domestic cat (Conchou et al., 2012). Terrestrial, freshwater, and marine carnivorans (including pinnipeds, mustelids, ursids, and procyonids) were investigated using high-resolution CT data, revealing more complex maxilloturbinals and less complex ethmoturbinals for the aquatic species (compared to terrestrial species) in order to better conserve heat and water in an aquatic environment (Van Valkenburgh et al., 2011). Additional studies that included the artic fox, kit fox, red fox, grey fox, coyote, grey wolf, African wild dog, and bush dog showed that a branching maxilloturbinal is found in all canids examined to date (Green et al., 2012; Van Valkenburgh et al., 2014a; Van Valkenburgh et al., 2004). Likewise, some felids possess a scrolled maxilloturbinal, as displayed by studies that broadened felid nasal investigation to incorporate the lion, leopard, cheetah, puma, bobcat, African wild cat, and ocelot (Van Valkenburgh et al., 2014a; Van Valkenburgh et al., 2004). Green (2012) also considered the sister group Arctoidea (ursids, mustelids, mephitids, procyonids, and pinnipeds) when examining the impact of latitudinal location and diet on respiratory and olfactory surface area in the nasal cavity.

Nasal anatomy and morphology of mammalian species of the order Rodentia have been studied extensively. To date, the most detailed investigation on sciurid nasal anatomy and morphology showed a branching maxilloturbinal in the eastern gray squirrel that is much more complex than the maxilloturbinal in most other rodents (Richter et al., in preparation). Further

studies investigating rodent nasal anatomy and morphology include the mouse (Adams, 1972; Gross et al., 1982; Jacob & Chole, 2006; Mery et al., 1994), rat (Adams et al., 1991; Bojsen-Moller, 2004; Bojsen-Moller & Fahrenkrug, 1971; Kimbell et al., 1997; Mery et al., 1994; Schreider & Raabe, 1981; Schroeter et al., 2012), guinea pig (Schreider & Hutchens, 1980), and hamster (Adams et al., 1991; Adams & McFarland, 1972). Other than the study on the eastern gray squirrel (Richter et al., in preparation), little information can be found regarding the nasal anatomy and morphology of sciurid species, despite accounting for the third largest family in the order Rodentia (Carleton & Musser, 2005). However, the study by Richter et al. (in preparation) has shown that the eastern gray squirrel boasts a more complex nasal cavity compared to other rodent species.

Of the three orders of Mammalia considered in this study, it is evident from available literature that the least nasal morphological data is available for species of the order Ungulata. Even though ungulates comprise the largest prey species, nasal form and function in these animals remain relatively uninvestigated compared to carnivores and rodents (Ranslow et al., 2014). A study by Ranslow et al. (2014) showed that the white-tailed deer possesses simpler maxilloturbinals, but very complex ethmoturbinals when compared to carnivores. Further, sixty-three species of bovids were examined using X-ray CT data in the "most comprehensive quantitative analysis of sinus morphology ever attempted" (Farke, 2010). MRI data were used to advance veterinary diagnoses in relation to horse nasal anatomy (Arencibia et al., 2000; Kumar et al., 2000). Other ungulate species that have been examined include the goat (Kumar et al., 1993), tapir (Witmer et al., 1999), and antelope (Kamau et al., 1984).

The objective of this work is to compare nasal anatomy, morphometry, and functional morphology across species using high-resolution MRI and state-of-the-art anatomical

reconstruction and morphometric analysis techniques (Craven et al., 2007; Van Valkenburgh et al., 2004). Though qualitative comparative studies of nasal anatomy have been performed (most notably by Sir Victor Negus (1956; 1958)), a quantitative comparison of nasal form and function across species is lacking. Here, we qualitatively and quantitatively compare the nasal cavity in the following species: house mouse (*Mus musculus*), eastern gray squirrel (*Sciurus carolinensis*), sea otter (*Enhydra lutris*), bobcat (*Lynx rufus*), coyote (*Canis latrans*), domestic dog (*Canis familiaris*), and white-tailed deer (*Odocoileus virginianus*). Of these mammals, the dog, coyote, bobcat, and sea otter are all carnivores; the eastern gray squirrel and the mouse are rodents; and the white-tailed deer is an ungulate. In regards to these species, the carnivores are predators; the rodents are primarily prey, but Callahan (1993) notes that sciurid species do exhibit some predatory behaviors; and the ungulate is prey. Additionally, the sea otter is an aquatic mammal, spending most of its life in the water, while the remaining considered species are terrestrial. Qualitatively, airway cross-sections and three-dimensional anatomical reconstructions are shown for each specimen. Quantitative measures of nasal form (e.g., airway perimeter, cross-sectional area, surface area) are then compared across species and the functional implications of these data regarding respiratory and olfactory airflow are considered.

Chapter 2

Materials and Methods

Specimens

The species considered in this study (in order of increasing mass) include the mouse, eastern gray squirrel, sea otter, bobcat, coyote, domestic dog, and the white-tailed deer (Table 1). The mouse (*Mus musculus*) and domestic dog (mixed-breed Labrador retriever) specimens were acquired from biological supply companies (see Coppola et al., 2014 and Craven et al., 2007, respectively). The eastern gray squirrel (*Sciurus carolinensis*), bobcat (*Lynx rufus*), coyote (*Canis latrans*), and white-tailed deer (*Odocoileus virginianus*) specimens were acquired from hunters and trappers in Pennsylvania (PA) in accordance with regulations of the PA Game Commission. Finally, the sea otter (*Enhydra lutris*) specimen was obtained from the California Department of Fish and Wildlife. Preparation of the mouse, dog, and white-tailed deer specimens for MRI scanning has been previously described in detail (see Coppola et al., 2014; Craven et al., 2007; Ranslow et al., 2014). Preparation of the eastern gray squirrel, sea otter, bobcat, and coyote followed that of the white-tailed deer (Ranslow et al., 2014).

Table 1: Summary of specimens

Species	Sex	Mass (kg)	MRI Resolution (µm)
Mouse	F	0.0388	25x25x25
Eastern Gray Squirrel	F	0.418	40x40x40
Sea Otter	--	11.2	70x70x70
Bobcat	F	12.0	80x80x80
Coyote	F	14.5	150x150x150
Domestic Dog	F	29.5	180x180x200
White-tailed Deer	M	62.0	100x100x100

MRI

In order to image the air passages, each specimen remained in solution (distilled water for the dog and PBS/Magnevist solution for all other specimens) during MRI scanning (as previously described for the dog and white-tailed deer by Craven et al., 2007 and Ranslow et al., 2014, respectively). To remove air bubbles trapped inside the nasal cavity, a combination of low-frequency vibration, steady pumping of the fluid solution through the airway, and a partial vacuum was applied. Trapped air can be detrimental to MRI because it can cause signal voids, as well as local distortion of the scans due to magnetic susceptibility effects.

The MRI imaging for the eastern gray squirrel was conducted on a 14.1-Tesla vertical Agilent system (Agilent, Santa Clara, CA) using a 40 mm inner diameter millipede resonator. All remaining specimens were imaged on a 7-Tesla horizontal Agilent system using a 20 cm inner diameter quadrature driven birdcage resonator. For each of the specimens, since the length of the cadaver head was greater than the linear region of the magnetic field gradients, multiple overlapping composite scans were obtained to cover the entire length of the specimen to avoid image distortion at the end of the gradient set. Spatial resolutions ranging from 25 μm isotropic in the case of the mouse to 180 x 180 x 200 μm in the case of the domestic dog were attained. Table 1 provides a summary of the MRI spatial resolution obtained for each specimen. The resulting MRI data sets were processed and the nasal airway was segmented using Avizo (Visualization Sciences Group, USA).

Airway Reconstruction

The methodology for image processing, segmentation, and reconstruction of the MRI data for all specimens considered was performed as in Craven et al. (2007). In order to process the raw MRI data, a three-dimensional, edge-preserving median filter was applied to the images,

enabling the preservation of image edges as noise was removed. Subsequently, a linear contrast stretch in Avizo was then performed to further enhance each data set. This resulted in high-contrast image data with optimal quality for image segmentation.

Due to the bilateral symmetry of the nasal cavity, only one nasal airway was segmented for each specimen. For the mouse, the right nasal airway was segmented, whereas the left nasal airway was segmented for the remaining specimens. The specific airway segmented for each specimen was determined by selecting the airway with the fewest artifacts present in the MRI scans (e.g., fewer residual air bubbles that remained trapped in the nasal airway during imaging). The segmentation utilized a combination of both algorithmic and manual methods. As demonstrated in Craven et al. (2007) and Ranslow et al. (2014), segmentation of the large airways was performed using a variety of algorithmic schemes including region growing, thresholding, contour extraction by way of edge detection, and contour interpolation and extrapolation in the axial direction. However, segmentation of the smallest airways (e.g., only a few voxels in width), presented greater difficulty, as the airway/tissue interface is less distinct near the resolution threshold. Such airways required an interactive segmentation technique that varied from manual correction of the algorithmic segmentation to complete manual segmentation. The segmentation process resulted in a binary data set of voxels, where the airway was labeled as 1 and non-airway structures (e.g., bone, tissue) were labeled as 0.

Using the modified form of the marching cubes algorithm (Lorensen & Cline, 1987) available in Avizo, a three-dimensional triangulated surface model of the nasal airway walls was generated from the segmentation of each specimen. To eliminate surface "staircasing" (or castellation), the surface model was smoothed in Avizo by means of the smoothing algorithm of Taubin (1995), which avoids surface shrinkage. Comparisons of the internal volume of each

three-dimensional surface model before and after smoothing showed differences of less than 0.1%, thereby demonstrating that the smoothing algorithm did indeed prevent surface shrinkage.

Airway Morphometry and Functional Implications

For each specimen, a morphometric analysis of the nasal airway was conducted using custom image processing software in MATLAB (MathWorks, Natick, MA), which was developed and validated by Craven et al. (2007). The morphometry data included the airway perimeter (P) and cross-sectional area (A_c), determined from the segmented slices using the airway boundary and the total number of segmented airway pixels, respectively, along with the in-plane spatial resolution. Additional parameters that were obtained include the hydraulic diameter (D_h), cumulative surface area (A_s), and cumulative internal volume (V).

Equation 1 shows the definition of hydraulic diameter, which quantifies the mean airway gap width and is typically used to determine fluid flow characteristics in noncircular channels (Craven et al., 2007).

$$\boldsymbol{D_h = \frac{4A_c}{P}} \quad (1)$$

Calculating the cumulative surface area, especially of intricate three-dimensional structures such as the nasal airways considered in this study, is much more difficult and is obtained using Equation 2 and the trapezoidal rule to carry out the numerical integration.

$$\boldsymbol{A_s(z) = \int_0^z P(z)\sqrt{1 + \frac{1}{4}\left(\frac{dD_h}{dz}\right)^2}\, dz} \quad (2)$$

Likewise, integrating the cross-sectional area in the axial direction yields the cumulative internal volume of the nasal airway, as shown in Equation 3.

$$\boldsymbol{V(z) = \int_0^z A_c(z)dz} \quad (3)$$

The functional implications of the nasal airway morphometric data concerning respiration and olfaction rely on the dimensionless Reynolds (Re) and Womersley (Wo) numbers, as shown by Equations 4 and 5, respectively, where V_{ave} is the cross-sectional average velocity, ν is the kinematic viscosity of air, and f is the frequency of respiration or sniffing measured in Hertz.

$$\boldsymbol{Re_{Dh}} = \frac{\boldsymbol{V_{ave} D_h}}{\boldsymbol{\nu}} \quad (4)$$

$$\boldsymbol{Wo_{Dh}} = \frac{\boldsymbol{D_h}}{\boldsymbol{2}} \sqrt{\frac{\boldsymbol{2\pi f}}{\boldsymbol{\nu}}} \quad (5)$$

The Reynolds number, which is defined as the ratio of inertial to viscous forces in fluid flow, can be used to predict whether flow, in this case the nasal airflow, is laminar or turbulent. For steady or quasi-steady flow, a small Reynolds number ($Re_{Dh} < 2000$) generally designates laminar flow; a high Reynolds number indicates a transition to turbulent flow.

Likewise, the Womersley number indicates the degree of unsteadiness in the fluid flow (Loudon & Tordesillas, 1998). Typically, when the Womersley number is less than unity ($Wo_{Dh} < 1$), the flow is characterized as quasi-steady, signifying that the time-dependent solution at a given point in time is equivalent to the steady-state solution at the same flow rate. When the Womersley number increases above one, however, the flow gradually becomes unsteady, moving more and more towards fully transient flow with an increasing Womersley number.

To predict the existence of laminar or turbulent flow when the flow is fully transient ($Wo_{Dh} > 1$), the ratio of the maximum Reynolds number to the Womersley number, Re_{max}/Wo, is used. Considering oscillatory pipe flow, transition from laminar to turbulent flow occurs in the range of Re_{max}/Wo = 250-1000 (Peacock et al., 1998). However, disturbed flow from airway branching can cause transition to occur at lower values of this ratio (Peacock et al., 1998).

When calculating the Reynolds and Womersley numbers, it is essential to use physiologically realistic estimates of the volumetric airflow rate and frequency for both respiration and sniffing, which are shown in Table 2 for the specimens considered in this study. For respiration, volumetric airflow rate and frequency were calculated based on the mass of the specimen and allometric relationships provided by Bide et al. (2000) and Stahl (1967) for respiratory minute volume and rate, respectively. For sniffing, the volumetric flow rate was estimated using the mass of the specimen and the allometric relationship provided by Craven et al. (2010) for the mean inspiratory flow rate during sniffing in the domestic dog, the only such allometric data available in the literature for sniffing in non-primate mammals. The sniff frequency of the mouse was estimated based on data recorded by Wesson et al. (2008) for peak sustained frequency of sniffing in mice in odor-guided tasks. The sniff frequency of the eastern gray squirrel was estimated from sniffing measurements made by Youngentob et al. (1987) in rats of similar size. The sniff frequency for each of the remaining five species was estimated from the allometric and experimental data of Craven et al. (2010) for canine subjects of similar size and mass.

Table 2: Estimates of volumetric airflow rate and frequency for respiration and sniffing

		RESPIRATION		**SNIFFING**	
Species	**Mass (kg)**	**Volumetric Flow Rate (l/min)**	**Frequency (Hz)**	**Volumetric Flow Rate (l/min)**	**Frequency (Hz)**
Mouse	0.0388	0.036	2.08	0.0199	10[a]
Eastern Gray Squirrel	0.418	0.246	1.12	0.230	8[b,c]
Sea Otter	11.2	3.52	0.48	6.80	5[b]
Bobcat	12.0	3.73	0.47	7.30	5[b]
Coyote	14.5	4.34	0.44	8.88	5[b]
Domestic Dog	29.5	7.71	0.37	18.4	5[b]
White-tailed Deer	62.0	14.1	0.30	39.6	5[b]

[a] Wesson et al., 2008
[b] Craven et al., 2010
[c] Youngentob et al., 1987

Chapter 3

Results

Nasal Airway Anatomy

Overall, the general architecture of the mammalian nasal cavity is comparable across all species considered in this study. Likewise, comparisons to previous studies of other non-primate species (e.g., carnivores (Negus, 1958; Evans, 1993; Van Valkenburgh et al., 2004; Craven et al., 2007; Green et al., 2012), rodents (Adams & McFarland, 1972; Adams, 1972; Schreider & Raabe, 1981; Kimbell et al., 1997; Richter et al., in preparation), and ungulates (Ranslow et al., 2014)) verify the similarities present in nasal form and architecture. Moving caudally, the nasal cavity consists of three primary regions: nasal vestibule, maxilloturbinal, and ethmoidal. A transitional region, known as the nasomaxillary region, is found between the maxilloturbinal and ethmoidal regions, where the nasomaxillary opening is located ventrally. The ethmoidal region is isolated to a posterosuperior region known as the olfactory recess, which is separated from the primary respiratory pathway by a bony plate known as the *lamina transversa* (Craven et al., 2010). Finally, as seen in the three-dimensional anatomical reconstructions of the nasal fossae (Figure 2), in each species the dorsal meatus directly connects the nasal vestibule to the ethmoidal region, suggesting that it serves as a bypass for odorant-laden airflow around the complex maxilloturbinal region.

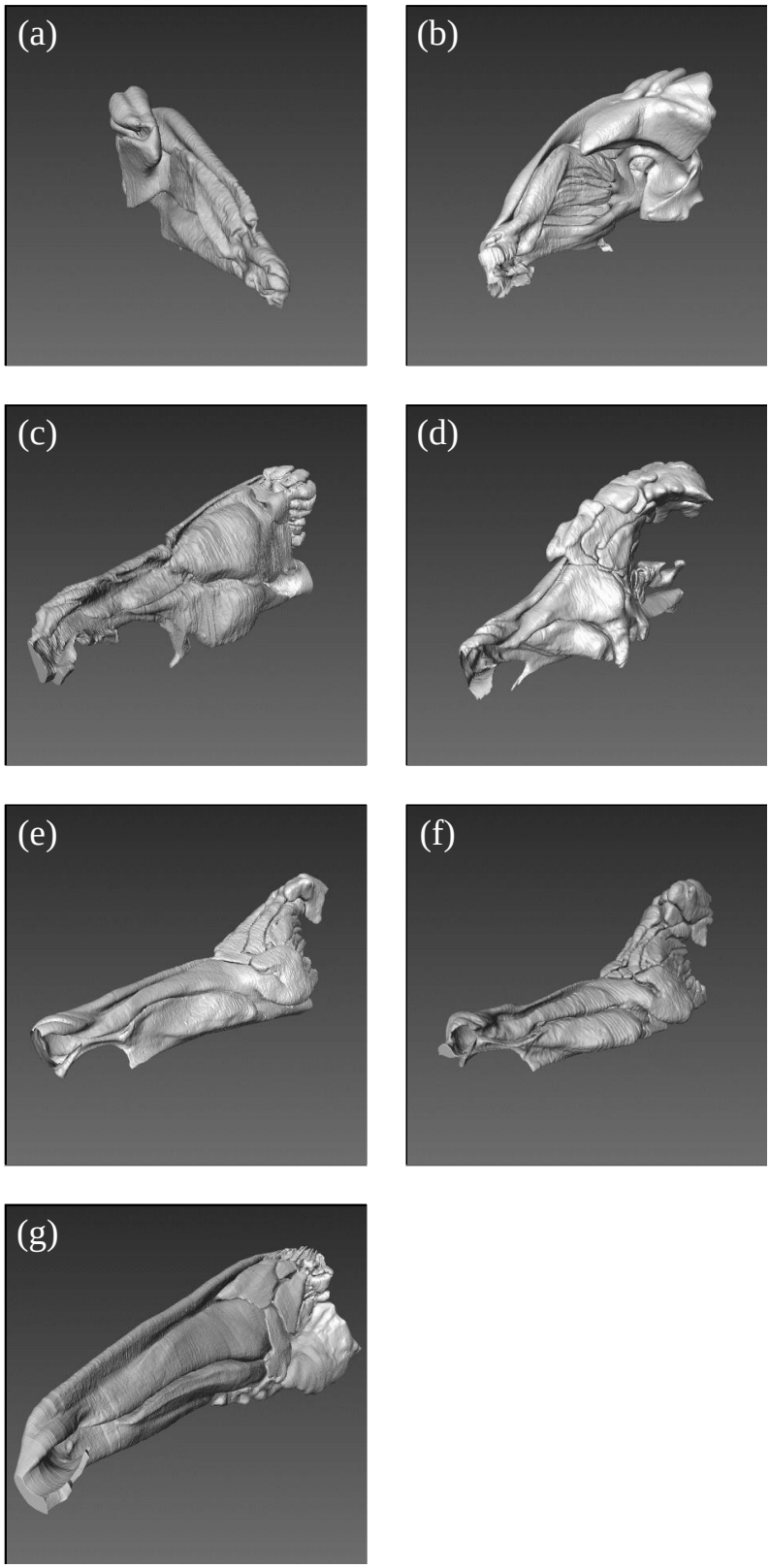

Figure 2: Three-dimensional anatomical reconstruction of the nasal airway of the (a) mouse, (b) eastern gray squirrel, (c) sea otter, (d) bobcat, (e) coyote, (f) domestic dog, and (g) white-tailed deer.

Within mammalian nasal anatomy, four different types of turbinals exist (in increasing order of complexity): single-scroll, double-scroll, folded, and branching (Negus, 1958). Analysis of the cross-sectional anatomy allows for the identification of each turbinal type for each specimen considered in this study. Figures 3-9 show transverse airway cross-sections of a single nasal airway in the mouse, eastern gray squirrel, sea otter, bobcat, coyote, domestic dog, and white-tailed deer. Frequently, the maxilloturbinal is the most complicated region within the nasal fossa as it provides a large surface area for respiratory heat and moisture exchange. According to Negus (1958), rodents tend to possess a single-scroll, double-scroll, or folded maxilloturbinal. This was partially confirmed by the present results. The maxilloturbinal in the mouse (Figure 3) is seen to be of the single-scroll type, consistent with previous studies (Adams, 1972; Mery et al., 1994), and similar to that of other rodents such as the rat (Mery et al., 1994; Schreider & Raabe, 1981). The eastern gray squirrel (Figure 4), however, is seen to possess a branching maxilloturbinal, which interestingly contradicts Negus (1958), who described sciurid species as having a folded maxilloturbinal. Thus, the maxilloturbinal of the eastern gray squirrel is much more complex than most other rodents, which typically possess a single- or double-scroll maxilloturbinal.

Carnivores generally possess an extremely complex branching (e.g., canids (Evans, 1993; Van Valkenburgh et al., 2004; Craven et al., 2007; Green et al., 2012), arctoids (Van Valkenburgh et al., 2011; Green et al., 2012)) or folded (e.g., felids (Van Valkenburgh et al., 2004)) maxilloturbinal. As shown in Figure 5, the sea otter possesses the most intricate maxilloturbinal of all the species considered in the present study, which is consistent with the observations of Negus (1958) and Van Valkenburgh et al. (2011) in the sea otter and other aquatic carnivores (e.g., grey seal, leopard seal). This increased complexity is required to provide

a large respiratory surface area to meet the increased demands for heat and water conservation in an aquatic environment (as compared to a terrestrial environment).

The coyote (Figure 7) and the domestic dog (Figure 8) are shown to possess a branching maxilloturbinal that is extremely similar between the two animals. While canids have a complex branching maxilloturbinal that has a "dendritic appearance," the maxilloturbinal of felids is generally of the folded type (Van Valkenburgh et al., 2004). This is confirmed in Figure 6, where the bobcat appears to possess an elaborately folded maxilloturbinal.

The white-tailed deer (Figure 9), which is the only ungulate considered in this study, possesses a maxilloturbinal of the double-scroll variety, typical of most ungulates (Negus, 1958; Ranslow et al., 2014). Despite being the largest specimen considered, the white-tailed deer displays one of the simpler maxilloturbinal structures compared to the other specimens. Only the maxilloturbinal of the mouse is less anatomically complex.

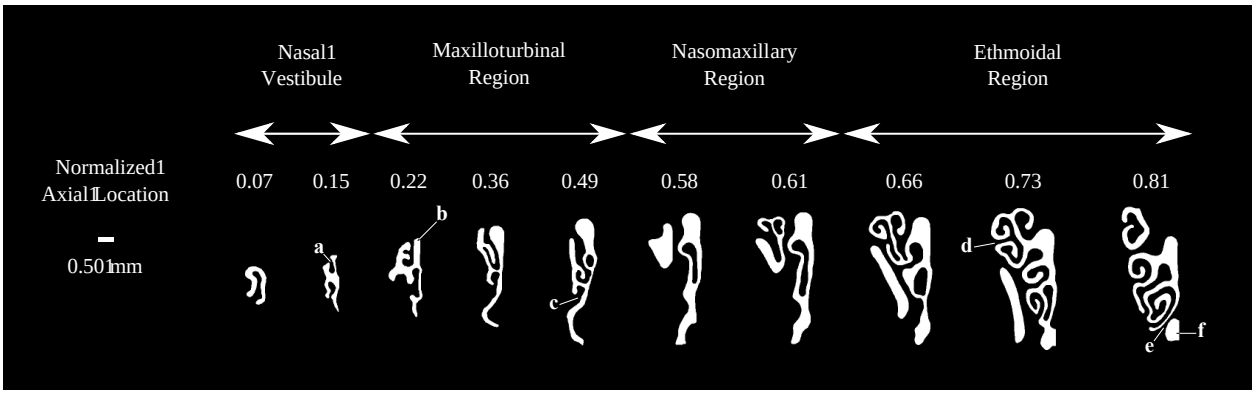

Figure 3: Transverse airway cross-sections of the right nasal airway of the mouse at various axial locations throughout the nasal fossa. Axial location is normalized by the total length of the nasal airway, 1.25 cm. a, nasoturbinal; b, dorsal meatus; c, maxilloturbinal; d, ethmoturbinals; e, lamina transversa; f, nasopharynx.

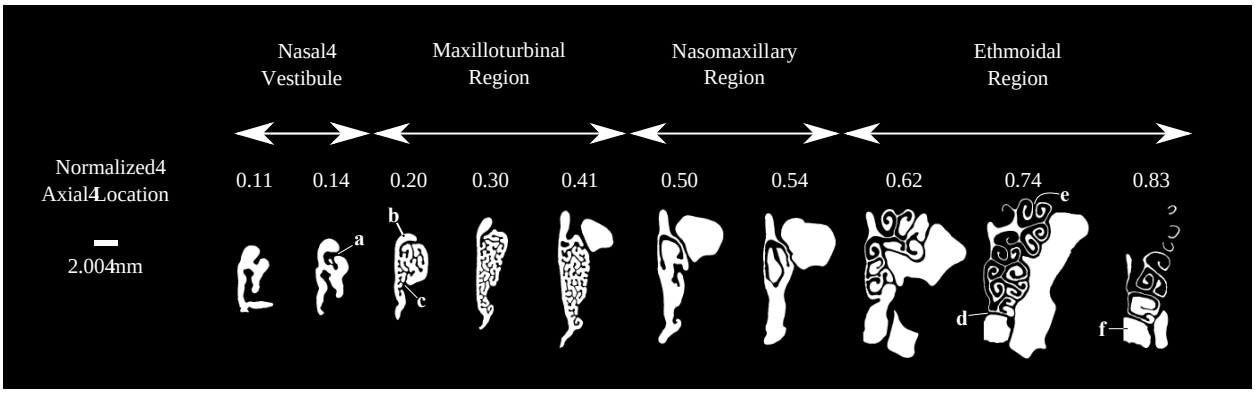

Figure 4: Transverse airway cross-sections of the left nasal airway of the eastern gray squirrel at various axial locations throughout the nasal fossa. Axial location is normalized by the total length of the nasal airway, 3.04 cm. a, nasoturbinal; b, dorsal meatus; c, maxilloturbinal; d, lamina transversa; e, ethmoturbinals; f, nasopharynx.

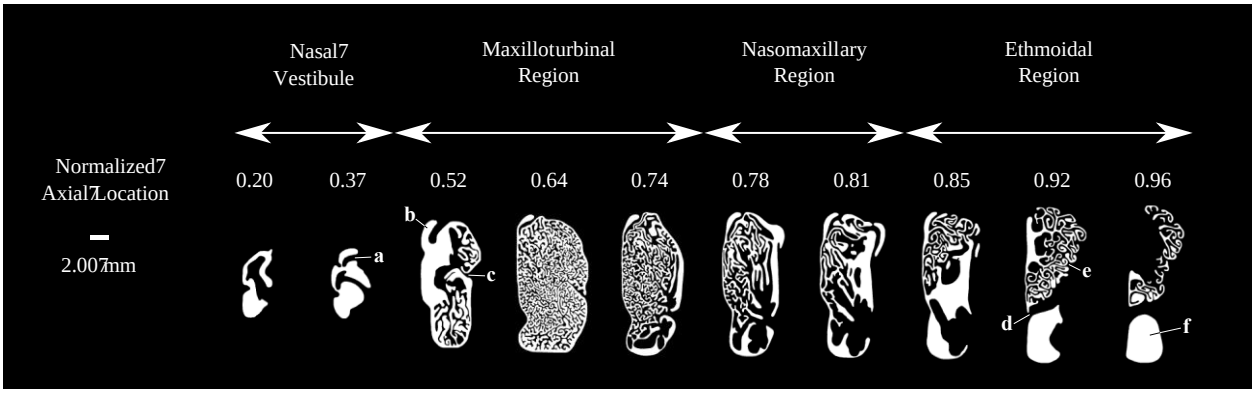

Figure 5: Transverse airway cross-sections of the left nasal airway of the sea otter at various axial locations throughout the nasal fossa. Axial location is normalized by the total length of the nasal airway, 7.36 cm. a, nasoturbinal; b, dorsal meatus; c, maxilloturbinal; d, lamina transversa; e, ethmoturbinals; f, nasopharynx.

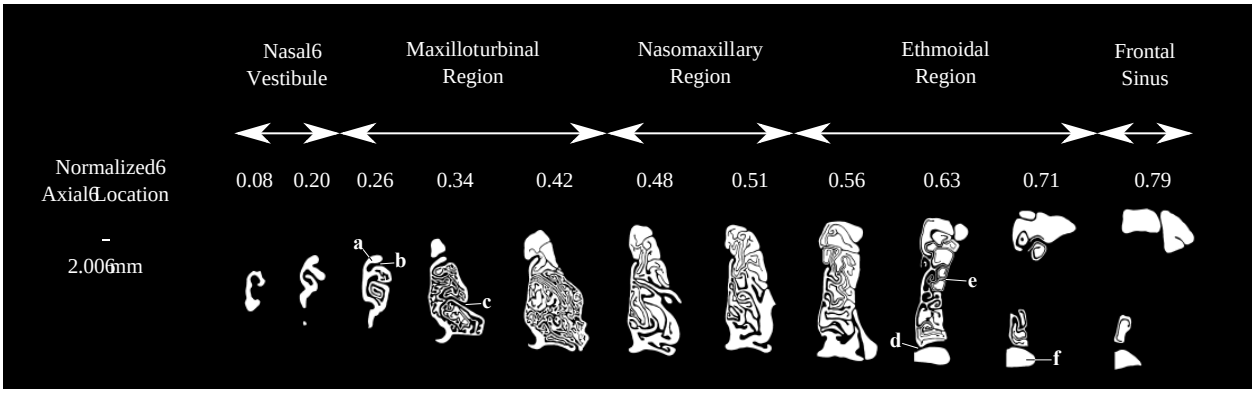

Figure 6: Transverse airway cross-sections of the left nasal airway of the bobcat at various axial locations throughout the nasal fossa. Axial location is normalized by the total length of the nasal airway, 8.78 cm. a, dorsal meatus; b, nasoturbinal; c, maxilloturbinal; d, lamina transversa; e, ethmoturbinals; f, nasopharynx.

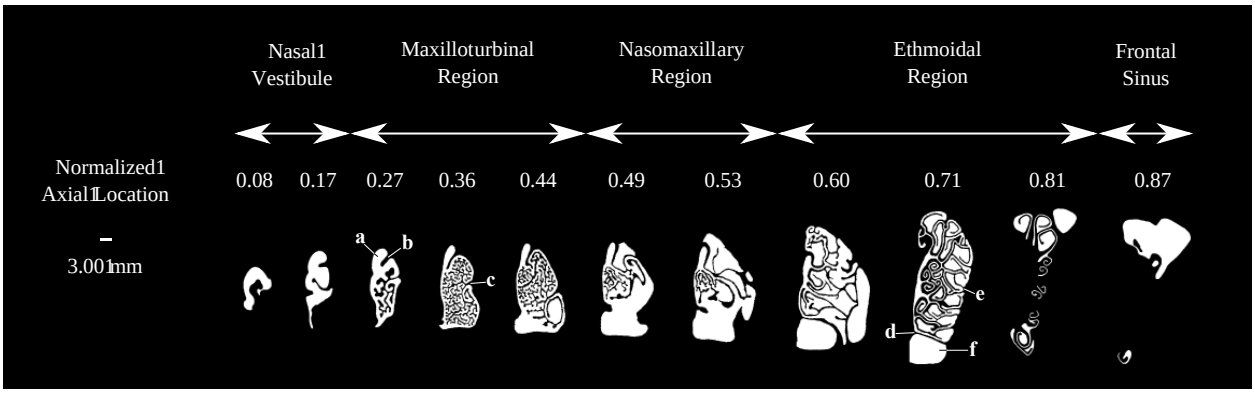

Figure 7: Transverse airway cross-sections of the left nasal airway of the coyote at various axial locations throughout the nasal fossa. Axial location is normalized by the total length of the nasal airway, 14.21 cm. a, dorsal meatus; b, nasoturbinal; c, maxilloturbinal; d, lamina transversa; e, ethmoturbinals; f, nasopharynx.

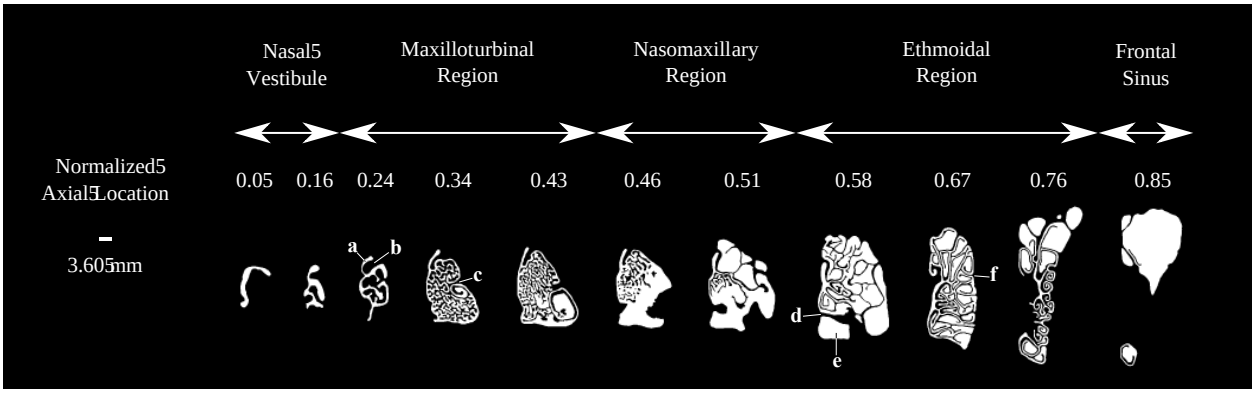

Figure 8: Transverse airway cross-sections of the left nasal airway of the domestic dog at various axial locations throughout the nasal fossa. Axial location is normalized by the total length of the nasal airway, 13.34 cm. a, dorsal meatus; b, nasoturbinal; c, maxilloturbinal; d, lamina transversa; e, nasopharynx; f, ethmoturbinals.

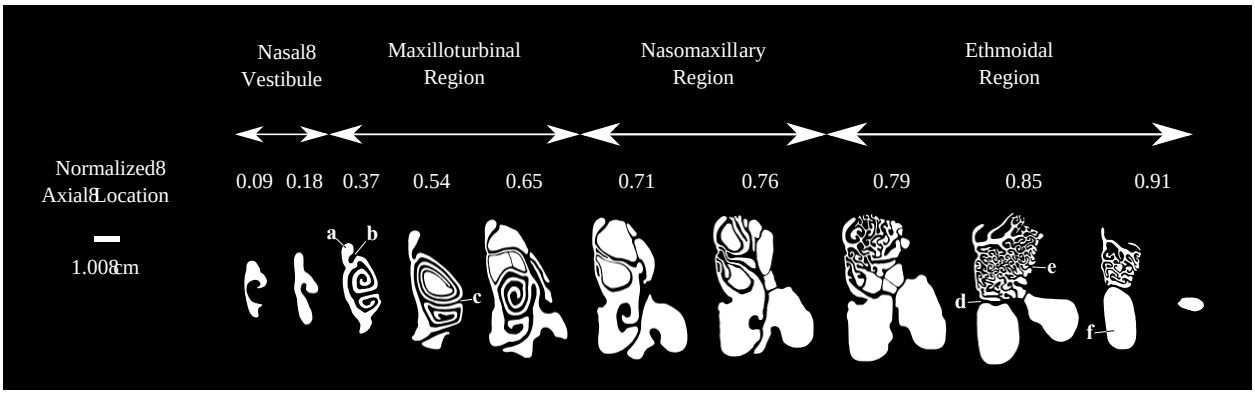

Figure 9: Transverse airway cross-sections of the left nasal airway of the white-tailed deer at various axial locations throughout the nasal fossa. Axial location is normalized by the total length of the nasal airway, 18.05 cm. a, dorsal meatus; b, nasoturbinal; c, maxilloturbinal; d, lamina transversa; e, ethmoturbinals; f, nasopharynx.

Interestingly, where some species lack in complexity, they compensate for in length. The total surface area of a region depends on both "the degree of branching," as well as the length (Negus, 1958). As in the case of some ungulates, a much greater snout length compared to carnivores gives rise to a longer turbinal (from naris to nasopharynx) relative to body size. The maxilloturbinal of the white-tailed deer is approximately 50% of the entire length of the nasal fossa (Ranslow et al., 2014). Even though the white-tailed deer possesses a far simpler double-scroll maxilloturbinal, the structure extends for a greater axial distance in order to increase surface area. For comparison, the maxilloturbinal of the coyote and domestic dog, both of which are complex branching structures, occupy approximately 27% and 30% of the nasal fossa, respectively.

In general, the ethmoidal region has a much simpler airway geometry than the complex maxilloturbinal region in most non-primate mammals. Most species possess single- or double-scroll ethmoturbinals. This is observed in the mouse, eastern gray squirrel, sea otter, bobcat, coyote, and domestic dog (see Figures 3-8). The white-tailed deer, however, is unlike most other non-primate species in that it possesses a much more complex folded ethmoturbinal organization compared to the typical single- and double-scroll ethmoturbinals (see Ranslow et al., 2014). The increased complexity of the ethmoturbinals in the white-tailed deer is evident in Figure 9. The complex folding may be a result of having a limited amount of space available for the ethmoidal region due to the elongated double-scroll maxilloturbinal. That is, the increased complexity of the folded ethmoturbinals of the white-tailed deer provides a large surface area for olfaction in a compact space.

Despite many anatomical parallels across the species considered here, distinct structural differences do exist. Most notably is the presence or the lack thereof of frontal sinuses, large

recesses that appear dorsocaudal to the ethmoidal region. Of the species considered in this study, the bobcat, coyote, and dog possess a frontal sinus (see Figures 6-8), which is consistent with the findings of Negus (1958) that species within the dog and cat families have such an arrangement. Conversely, the mouse, eastern gray squirrel, sea otter, and white-tailed deer lack a frontal sinus. Another distinct feature is the maxillary recess, which is seen in all of the terrestrial mammals considered here (mouse, eastern gray squirrel, bobcat, coyote, dog, and white-tailed deer). However, the aquatic sea otter does not possess a discernible maxillary recess. Perhaps this is a result of the increased complexity of the maxilloturbinal and a lack of available space within the snout.

Airway Morphometry

Morphometric analysis was performed for all specimens considered in this study by calculating the distribution of perimeter, cross-sectional area, hydraulic diameter, and cumulative surface area in the nasal airway. Further consideration included examining respiratory surface area, ethmoidal surface area, total internal volume, and total surface area with respect to body mass. For reference, see Figures 3-9 for the location of the different anatomical regions for each specimen.

Figure 10 contains plots of the airway perimeter versus normalized axial location. The relative distribution of perimeter varies between the seven species examined. In the eastern gray squirrel, coyote, dog, and white-tailed deer, there is a pronounced rise in perimeter progressing caudally through the maxilloturbinal region, a decrease to a local minimum in the nasomaxillary region, and an ensuing increase to the greatest airway perimeter in the ethmoidal region. The sea otter and bobcat differ slightly in the sense that the perimeter is largest in the maxilloturbinal regions, followed by a decrease to a local minimum in the nasomaxillary region, and a less

pronounced increase in the ethmoidal region. The substantial increase in perimeter in the sea otter's maxilloturbinal region can be explained by an increased complexity resulting from a greater need for heat and water conservation in an aquatic environment. Perhaps the dramatic increase in the bobcat is a result of an increased folding of the maxilloturbinal to compensate for a shorter snout length when compared to other terrestrial carnivores (e.g., coyote, dog) (Van Valkenburgh et al., 2014a). In the mouse, the airway perimeter gradually increases with distance from the naris until reaching the largest perimeter in the ethmoidal region.

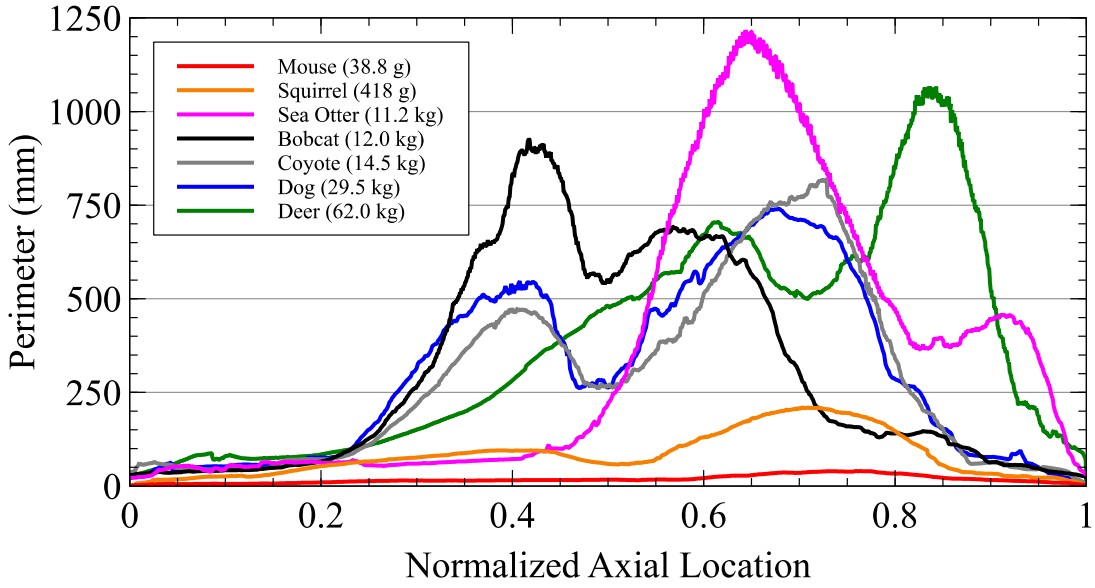

Figure 10: Distribution of perimeter versus normalized axial location. The greatest airway perimeter appears in the most convoluted regions of the nasal fossa (e.g., the maxilloturbinal region in the sea otter and the ethmoidal region in the white-tailed deer).

The distribution of cross-sectional area versus normalized axial location is shown in Figure 11. The mouse, eastern gray squirrel, and white-tailed deer all follow a similar pattern that reveals a steady increase in cross-sectional area to a maximum in the ethmoidal region due to a continual anteroposterior expansion of the nasal airway. The two canid species, coyote and dog, also reach a maximum cross-sectional area in the ethmoidal region. This is followed by a

decrease to a local minimum as the ethmoidal airways come to an end and a subsequent slight increase in cross-sectional area due to the frontal sinuses. The sea otter and bobcat follow similar patterns as seen with airway perimeter, in that the greatest cross-sectional area is reached in the maxilloturbinal region. The bobcat is similar to the other terrestrial carnivores in that, following the maximum cross-sectional area, a local minimum is observed in the nasomaxillary region, followed by a slight increase in cross-sectional area due to the emergence of the frontal sinuses.

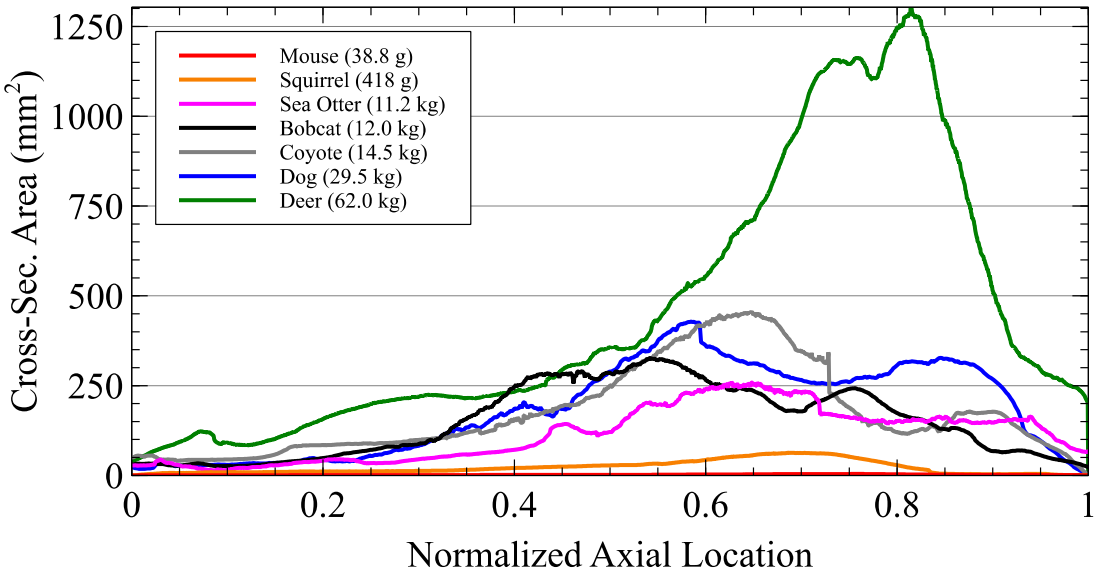

Figure 11: Distribution of cross-sectional area versus normalized axial location.

Figure 12 shows the distribution of hydraulic diameter, which is used to quantify the average airway gap width (Craven et al., 2007), versus normalized axial location. Sharp increases located in the most caudal portion of the nasal cavity for the bobcat, coyote, and dog appear as a result of the large frontal sinuses, which greatly increase the average airway gap width. Otherwise, it is interesting to note that, despite differences in body mass of over three orders of magnitude, the hydraulic diameter is quite comparable between all species in both the respiratory and olfactory regions. In both of these regions, the gap width is between

approximately 0.4 mm and 4 mm for all species. That is, hydraulic diameter only differs by approximately one order of magnitude, even though body size varies over three orders of magnitude. This may in part be due to functional constraints imposed on airway gap width by the underlying fluid dynamics and heat and mass transfer that occur in the nose, which are a function of the airway gap width.

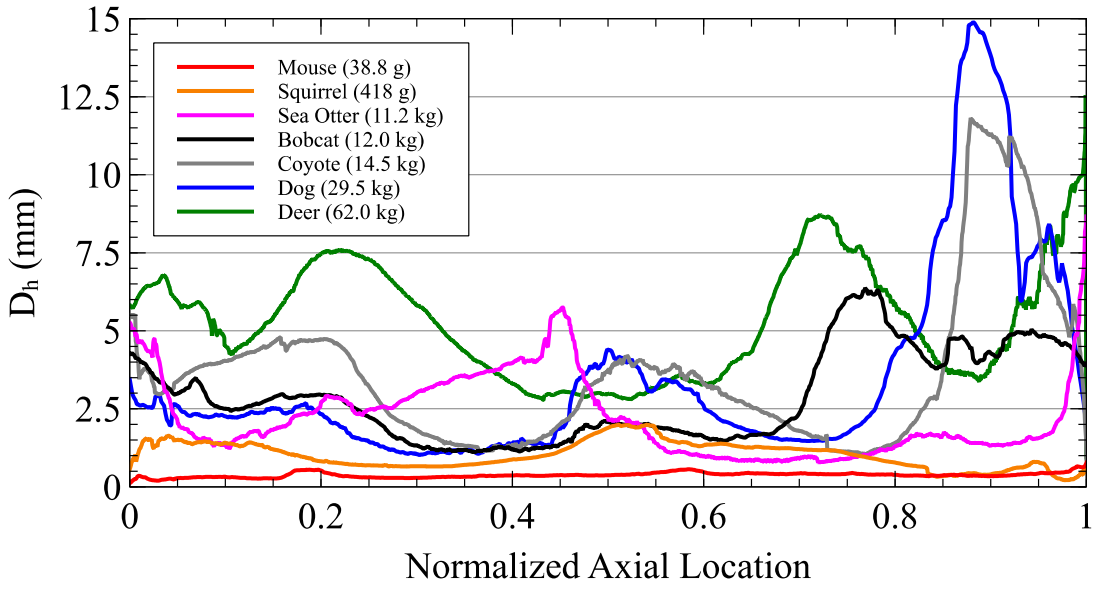

Figure 12: Distribution of hydraulic diameter versus normalized axial location. The hydraulic diameter, a measure of the mean airway gap width, is fairly comparable across all species in the respiratory and olfactory regions, ranging from about 0.4 mm to 4 mm, despite differences in body mass of over three orders of magnitude.

The distribution of cumulative surface area versus normalized axial location is plotted in Figure 13. Progressing caudally in all species, surface area increases, which can be a result of two separate factors: complexity and length of the nasal turbinals. An increase in either of these factors will increase surface area of the nasal airway, while an increase in both will have a compounding effect. While the sea otter and bobcat display similar total surface areas along comparable axial distances (7.36 cm and 8.78 cm, respectively), the cumulative surface area of

the sea otter begins to increase at a more caudal position when the maxilloturbinal starts to become increasingly complex. Unsurprisingly, the distribution of surface area in the coyote and dog is remarkably similar. Despite the simplicity of the double-scroll maxilloturbinal of the white-tailed deer, the total surface area is significantly greater than in the other species due to the increased length of the deer's nasal fossa.

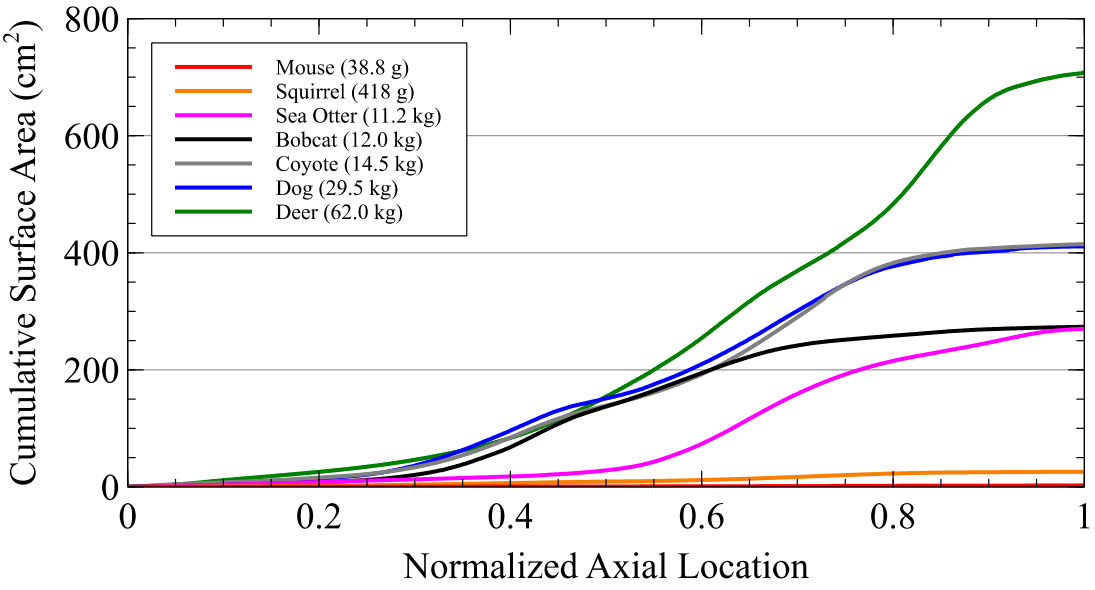

Figure 13: Distribution of cumulative surface area versus normalized axial location. Both increased complexity and greater length of the nasal turbinals increase surface area.

Plotted in Figure 14 is the total surface area of a single nasal airway versus body mass. The total surface area includes both respiratory and ethmoidal surface area. In the species considered in the present study, total nasal surface area is positively allometric with an allometric exponent of 0.78. Interestingly, despite being twice the size of the coyote, the domestic dog possesses a comparable total surface area. This may be due to differences in body composition (e.g., body fat) between the wild coyote and domestic dog specimens, and/or a reduction in the nasal surface area in the domesticated animal.

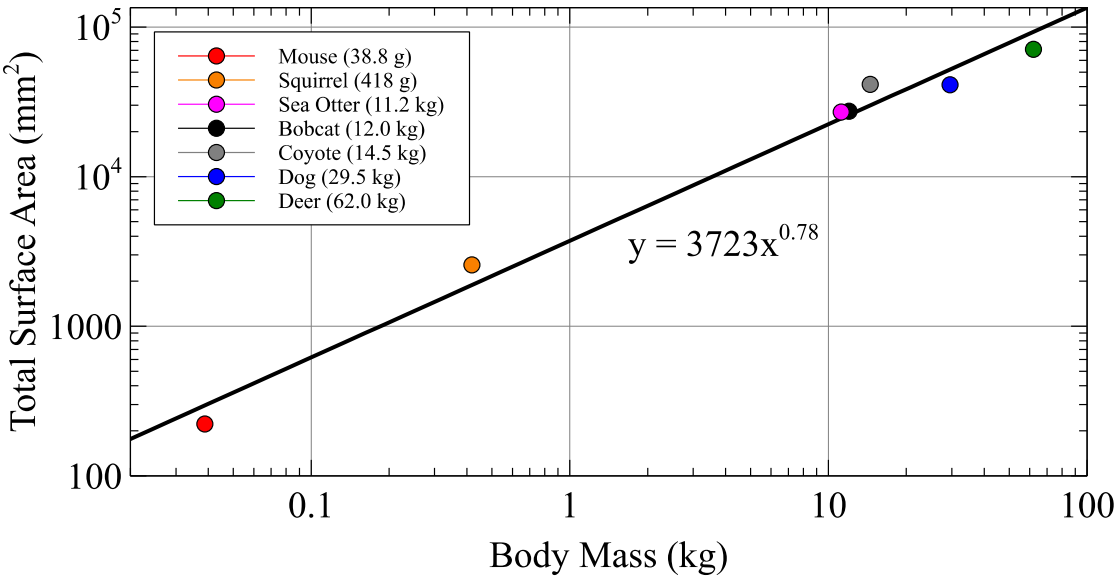

Figure 14: Total surface area versus body mass. Total surface area scales allometrically with body mass, with an allometric exponent of 0.78.

Respiratory surface area versus body mass is shown in Figure 15. The allometric exponent of the respiratory surface area (0.83) is roughly equivalent to the allometric exponent (0.809) for respiratory flow rate (i.e., respiratory minute volume – see Bide et al., 2000). This is likely due to the linear relationship between total heat/mass transfer and surface area. It is also interesting to note the two animals that are outliers from the best-fit regression line: the sea otter and domestic dog. Specifically, the sea otter possesses a significantly greater respiratory surface area relative to body mass, which is likely a result of the increased complexity of the maxilloturbinal in order to enhance heat and moisture exchange in an aquatic environment (Van Valkenburgh et al., 2011). Conversely, the domestic dog possesses significantly less respiratory surface area for its size compared to the other animals.

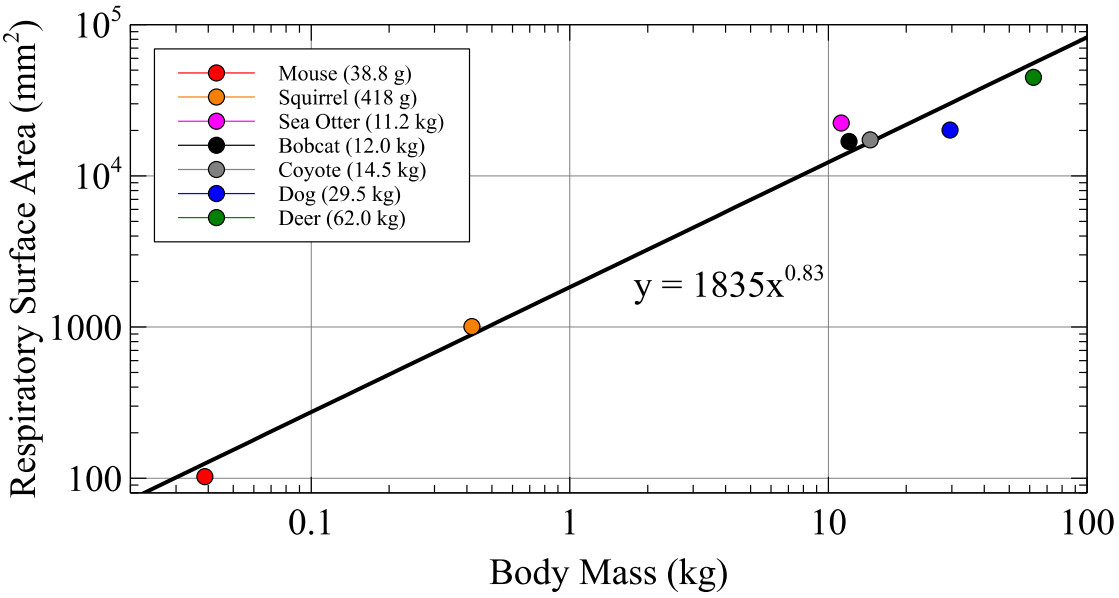

Figure 15: Respiratory surface area versus body mass. Respiratory surface area scales allometrically with body mass, with an allometric exponent of 0.83 (comparable to the allometric exponent for respiratory flow rate).

Ethmoidal surface area versus body mass is shown in Figure 16. It is important to note that ethmoidal surface area does not necessarily equal olfactory surface area (the area of the nasal fossa that is lined with olfactory epithelium). This distinction can only be made if the distribution of olfactory epithelium in the nose is mapped (e.g., using histological analysis techniques), which is beyond the scope of the present study but is a topic of future work. The allometric exponent for the ethmoidal surface area (0.72) is less than the allometric exponent for respiratory surface area (0.83). This means that, compared to respiratory surface area, smaller species (e.g., mouse, eastern gray squirrel) boast relatively greater ethmoidal surface area for their size compared to larger species (e.g., dog, white-tailed deer). One notable outlier seen in Figure 16 is the significant reduction in ethmoidal surface area of the sea otter, which is likely due to a decreased reliance on olfaction in an aquatic environment, as previously noted by Van Valkenburgh et al. (2011). Further, the coyote possesses a much greater ethmoidal surface area

for its size compared to the other species, perhaps due to an increased reliance on olfaction. In comparison to the domestic dog, from Figures 7 and 8, the coyote appears to possess a slightly larger dorsal meatus, which might convey a larger volume of air to the ethmoidal region, requiring a larger ethmoidal surface area for odorant uptake. Thus, it may be that over thousands of years of domestication, the ethmoidal surface area of the domestic dog has diminished compared to wild canid species, which rely on olfaction for survival.

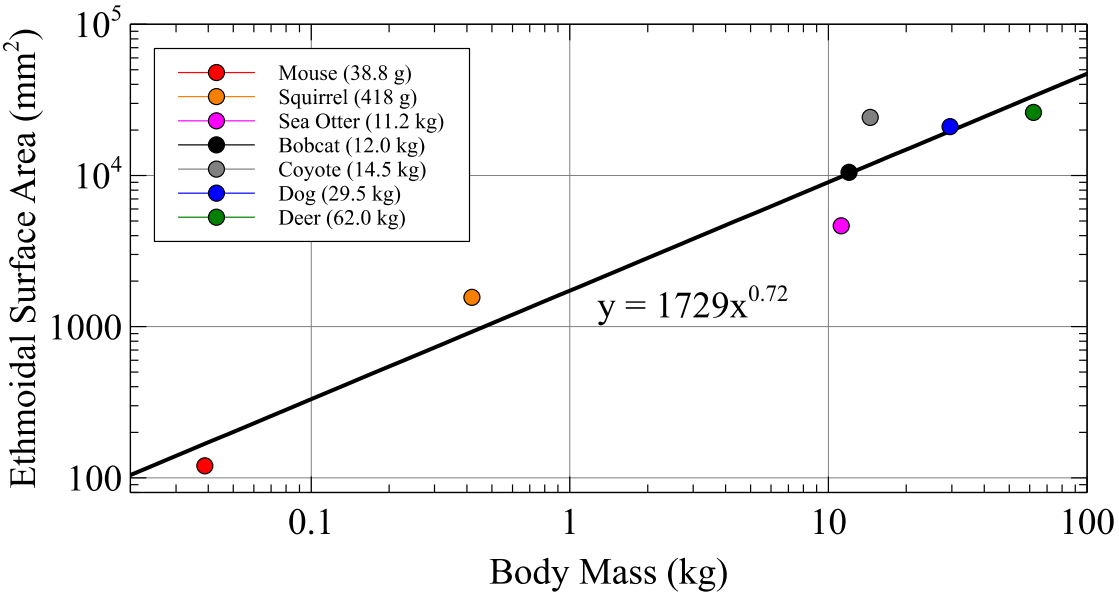

Figure 16: Ethmoidal surface area versus body mass. Ethmoidal surface area scales allometrically with body mass, with an allometric exponent of 0.72.

Finally, the total internal volume of the nasal fossa versus body mass is shown in Figure 17. As seen in the plot, total internal volume scales approximately isometrically (i.e., exponent of 1.06). That is, in contrast to surface area, the internal volume of the nasal fossa is directly proportional to the mass of the specimen.

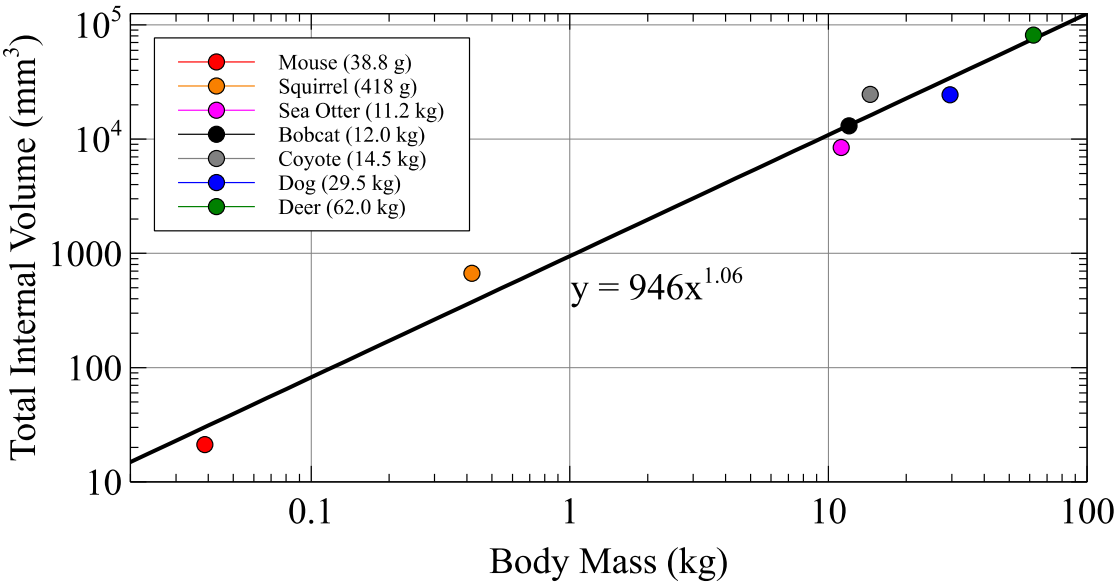

Figure 17: Total internal volume versus body mass. Total internal volume scales isometrically with body mass, with an allometric exponent of 1.06.

Functional Implications

Functionally, the Reynolds number is used to predict whether flow is laminar or turbulent. For steady or quasi-steady flow, a Reynolds number of less than 2000 generally indicates laminar flow, while a higher Reynolds number indicates a transition to turbulent flow. Figure 18 shows the distribution of the Reynolds number as a function of normalized axial location for steady respiration and sniffing flow rates in each specimen. Reynolds numbers are not shown beyond the location of the nasopharynx (i.e., ethmoidal and frontal sinus regions) because it is not presently known how much flow exits the nasal cavity via the nasopharynx and how much flow continues into the ethmoidal region. The mouse, eastern gray squirrel, sea otter, bobcat, and coyote all have Reynolds numbers well below 2000 for both steady respiration and sniffing flow rates. This indicates that nasal airflow in these species is likely to be laminar under steady or quasi-steady flow conditions. While airflow at steady respiratory flow rates in both the

dog and white-tailed deer appears to be laminar ($Re_{Dh} < 2000$), steady airflow at sniffing flow rates is in the transitional/turbulent regime in the vestibule and in the laminar regime elsewhere. Functionally, transitional or turbulent airflow may assist in mixing odorant-laden air in the nasal vestibule to ensure that some odorant reaches the dorsal meatus and is subsequently conveyed to the ethmoidal region where chemical sensing occurs.

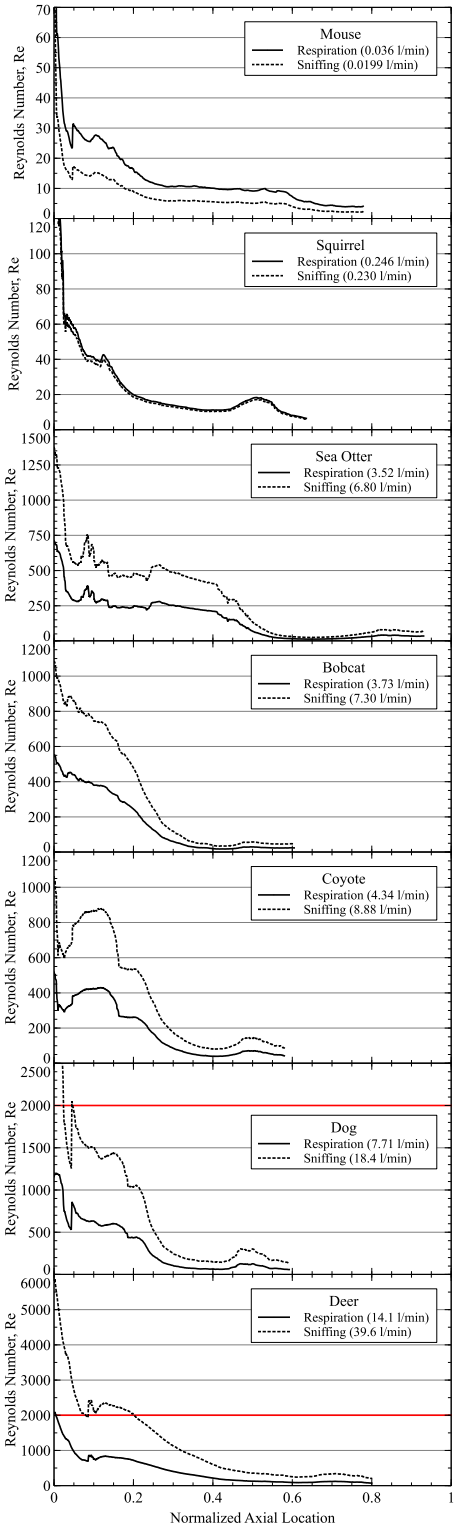

Figure 18: Distribution of the Reynolds number versus normalized axial location in a single nasal airway for steady respiration and sniffing flow rates. Axial location is normalized by the total length of the nasal airway. The red line delineates Re_{Dh} = 2000, the approximate value at which laminar-to-turbulent transition occurs for steady and quasi-steady flow.

The distribution of the Womersley number during respiration and sniffing for each specimen is plotted in Figure 19. Functionally, the Womersley number is used to evaluate the degree of unsteadiness in the flow. A Womersley number that is less than unity ($Wo_{Dh} < 1$) indicates quasi-steady flow; when the Womersley number is greater than one, flow becomes increasingly unsteady. The mouse is the only species considered in which the Womersley number for both respiration and sniffing is less than one, indicating quasi-steady flow throughout the entire nasal fossa of the mouse. For the eastern gray squirrel, the Womersley number is less than one for respiration throughout the entire nasal fossa; for sniffing, the Womersley number is greater than one in the nasal vestibule, the nasomaxillary region, and the anterior portion of the ethmoidal region. It is expected that the flow is slightly unsteady in these regions where the Womersley number is greater than one. During respiration, the sea otter shows a Womersley number that is less than one for the vast majority of the nasal cavity. A small portion of the maxilloturbinal region has a value slightly above one, where the flow might be slightly unsteady. During sniffing, the Womersley number is moderately greater than one in the nasal vestibule and the anterior portion of the maxilloturbinal region of the sea otter, indicating unsteady flow in these regions. The Womersley number does slightly increase above one in a small portion of the ethmoidal region, indicating that the flow might be slightly unsteady there. During respiration in the bobcat, the Womersley number is slightly greater than one in the caudal aspect of the ethmoidal region and the frontal sinus region due to the emergence of the frontal sinuses. During sniffing, the Womersley number is greater than one throughout the majority of the nasal fossa (a slight decrease below one occurs in the anterior half of the maxilloturbinal region). In the regions of the bobcat where the Womersley number is significantly greater than one, unsteady flow is to be expected. During respiration in the coyote, the Womersley number is less than one

everywhere except in the frontal sinus region. During sniffing, however, the magnitude of the Womersley number is greater than one in all regions except for a small portion in the middle of the maxilloturbinal region and the posterior aspect of the ethmoidal region. In these regions where the Womersley number is greater than one, the airflow is expected to be unsteady. The dog experiences similar Womersley number distributions as in the coyote. During respiration, Womersley numbers of greater than one are restricted to the frontal sinus region. During sniffing, the Womersley number is greater than one in all regions of the nasal fossa except for most of the maxilloturbinal region. Finally, during respiration in the white-tailed deer, the Womersley number is slightly greater than one throughout much of the anterior one-third of the nose and most of the nasomaxillary region, indicating slightly unsteady flow in these regions. For sniffing, the Womersley number throughout the entire nasal fossa is moderately greater than one, indicating unsteady flow.

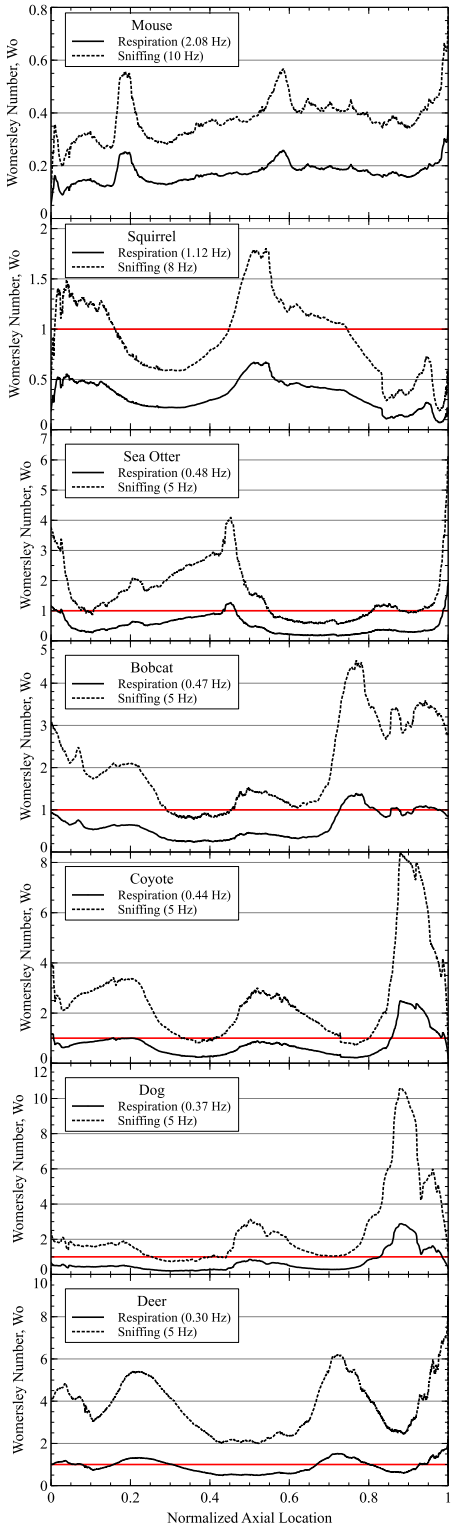

Figure 19: Distribution of the Womersley number versus normalized axial location in a single nasal airway for respiration and sniffing. Axial location is normalized by the total length of the nasal airway. The red line delineates Wo = 1, below which the flow is quasi-steady and above which the flow increasingly becomes unsteady.

When the flow is unsteady (Wo > 1), a more accurate prediction of laminar or turbulent flow uses the ratio of the maximum Reynolds number to the Womersley number, Re_{max}/Wo (see *Materials and Methods* for discussion). If the magnitude of the Womersley number is less than one (i.e., quasi-steady flow), this ratio is not considered, as the Reynolds number alone is sufficient for predicting the existence of laminar or turbulent flow. The results of the distribution of Re_{max}/Wo are shown in Figure 20 (like the plot for Reynolds number, values beyond the location of the nasopharynx are not shown). For unsteady flow, laminar-to-turbulent transition occurs in the range Re_{max}/Wo = 250-1000 (Peacock et al., 1998). Generally, for the specimens that experience unsteady airflow, the flow is mostly transitional or turbulent in the nasal vestibule and anterior maxilloturbinal region, yet some exceptions do exist. For the eastern gray squirrel, during sniffing, when we expect slightly unsteady airflow, the flow will likely be laminar ($Re_{max}/Wo < 250$). In the anterior half of the nasal fossa of the sea otter, where we expect unsteady airflow during sniffing, Re_{max}/Wo is greater than 250 in the nasal vestibule, indicating that the flow is likely to be transitional or turbulent. Progressing caudally into the maxilloturbinal region, Re_{max}/Wo drops below 250, indicating a reverse transition from turbulent flow to laminar flow. During sniffing, the bobcat experiences flow similar to the sea otter in that Re_{max}/Wo is greater than 250 in the nasal vestibule, indicating transitional or turbulent flow. This is followed by a decrease in Re_{max}/Wo below 250 in the maxilloturbinal region, indicating a reverse transition to laminar flow. Likewise, when the coyote undergoes bouts of sniffing, turbulent flow is only seen within the nasal vestibule. For the dog, during sniffing, when the flow is predicted to be unsteady, turbulent flow ($Re_{max}/Wo > 250$) extends through the nasal vestibule and slightly into the anterior portion of the maxilloturbinal region. Lastly, the white-tailed deer is predicted to experience unsteady flow in portions of the nasal fossa during respiration, and in the

entire nasal fossa during sniffing. During respiration, much of the anterior one-third of the nose (primarily the nasal vestibule) will likely experience transitional or turbulent flow, as Re_{max}/Wo is greater than 250. Progressing caudally, Re_{max}/Wo decreases below 250 at approximately the midpoint of the nasal fossa, indicating that the flow is expected to "relaminarize" (i.e., reverse transition to laminar flow). During sniffing, when the flow is predicted to be highly unsteady throughout the entire nasal fossa, the airflow is expected to be turbulent or transitional in the nasal vestibule and the anterior maxilloturbinal region and laminar elsewhere.

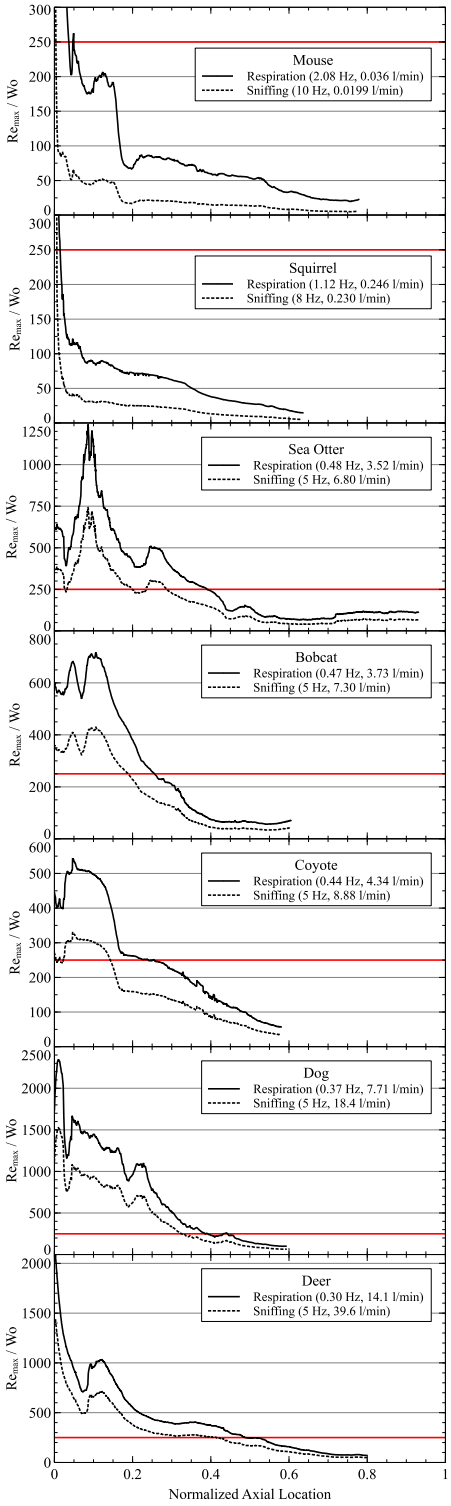

Figure 20: Distribution of the ratio of maximum Reynolds number to Womersley number for oscillatory nasal airflow versus normalized axial location in a single nasal airway for respiration and sniffing. Axial location is normalized by the total length of the nasal airway. The red line delineates $Re_{max}/Wo = 250$, the minimum value at which laminar-to-turbulent transition occurs for oscillatory pipe flow – see *Materials and Methods*.

Chapter 4

Summary, Conclusions, and Future Work

Summary

This study presented a qualitative and quantitative comparison of the anatomy and functional morphology of the mammalian nasal cavity using high-resolution MRI and state-of-the-art anatomical reconstruction techniques. Species investigated span three orders of the class Mammalia (Carnivora, Rodentia, Ungulata), and included the mouse, eastern gray squirrel, sea otter, bobcat, coyote, domestic dog, and white-tailed deer. Cross-sectional images of the nasal airway and three-dimensional anatomical reconstructions of the nasal cavity were presented. Advanced morphometric analysis techniques were used to quantitatively analyze measures of nasal form, including airway perimeter, cross-sectional area, and surface area. Finally, the implications of these data regarding respiratory and olfactory function were considered.

Conclusions

The conclusions of this work are summarized here in list form:

Nasal Airway Anatomy

1. The general architecture of the nasal cavity was comparable across all species considered in this study, and similar to other non-primate species previously studied.
2. MRI cross-sections of the nasal airway revealed the olfactory recess of each species to be isolated from the primary respiratory pathway by the *lamina transversa*. Three-dimensional anatomical reconstructions of each specimen showed the dorsal meatus

connecting the nasal vestibule directly with the ethmoidal region, indicating that the dorsal meatus likely serves as a conduit for odorant-bearing inspired air to bypass the convoluted respiratory region *en route* to the olfactory region.

3. Data show a variety of maxilloturbinal types present in the species considered. The mouse was shown to have a single-scroll maxilloturbinal, while the eastern gray squirrel possesses a maxilloturbinal of the branching type that is much more intricate than most other rodents. The sea otter, which was the only aquatic species investigated, was found to have a branching maxilloturbinal and the most complicated maxilloturbinal of all species examined. Similarly, the coyote and dog were discovered to possess a branching maxilloturbinal. Conversely, the last carnivore considered, the bobcat, was shown to have a folded maxilloturbinal. The white-tailed deer, and only ungulate in this study, was found to have a simpler maxilloturbinal of the double-scroll variety.
4. The length of a turbinal may compensate for the lack of complexity as seen with the extended, yet simpler, double-scroll maxilloturbinal of the white-tailed deer. The opposite is also true, as seen in the complex, folded maxilloturbinal of the bobcat, which possesses a relatively shorter snout.
5. All species considered in this study, except the white-tailed deer, were found to have single- and double-scroll ethmoturbinals. The white-tailed deer was shown to possess a much more complex folded set of ethmoturbinals, a unique trait when compared to most other non-primate species.
6. A frontal sinus region was present in the bobcat, coyote, and dog; a maxillary recess was seen in all terrestrial mammals, but a distinct maxillary recess was not identified in the aquatic sea otter.

Airway Morphometry

1. The greatest airway perimeter and cross-sectional area appear in the most convoluted regions of each animal (i.e., the maxilloturbinal and ethmoidal regions).
2. The hydraulic diameter (i.e., the average airway gap width) in both the respiratory and olfactory regions is quite comparable across species (ranges over approximately one order of magnitude, from about 0.4 mm to 4 mm) despite the fact that body mass varies over three orders of magnitude.
3. Surface area in the nasal cavity scales allometrically with body mass. The allometric exponent of the respiratory surface area (0.83) is greater than that of the ethmoidal surface area (0.72), indicating that, when compared to respiratory surface area, smaller species possess a relatively greater ethmoidal surface area for their size compared to larger species. The allometric exponent of the total nasal surface area is 0.78.
4. The total internal volume of the nasal fossa scales approximately isometrically with body mass.

Functional Implications

1. Functional parameters such as the Reynolds and Womersley numbers were used to predict laminar or turbulent and quasi-steady or unsteady flow, respectively.
2. In regions of unsteady airflow (where the Womersley number is greater than one), the ratio of the maximum Reynolds number to the Womersley number was used to more accurately predict laminar or turbulent flow.
3. Generally, when the flow was shown to be unsteady, turbulent (or transitional) flow was only found in the nasal vestibule and anterior maxilloturbinal region. The flow then "relaminarizes" as it flows caudally into regions with a smaller hydraulic diameter.

Future Work

Based on the results of this study, recommendations for future work include:

1. Exclusively relying on anatomical reconstruction of the nasal cavity is not enough to completely determine what accounts for greater olfactory ability (see Van Valkenburgh et al., 2014b). Complementary histological analyses of the nasal cavity are needed to investigate the distribution of olfactory and respiratory epithelium in the nose to truly quantify sensory and non-sensory surface area (e.g., as in Deleon & Smith, 2014). Further, mapping the respiratory and olfactory epithelium distribution on three-dimensional anatomical reconstructions will enhance these analyses (e.g., as in Deleon & Smith, 2014).
2. Conduct a comparative study of airflow and odorant deposition using computational fluid dynamics (CFD).
3. Validate the CFD simulation results with experimental measurements.

References

Adams, D. R. (1972). Olfactory and non-olfactory epithelia in the nasal cavity of the mouse, Peromyscus. *The American Journal of Anatomy*, *133*(1), 37–49.

Adams, D. R., Jones, A. M., Plopper, C. G., Serabjit-Singh, C. J., & Philpot, R. M. (1991). Distribution of cytochrome P-450 monoxygenase enzymes in the nasal mucosa of hamster and rat. *The American Journal of Anatomy*, *190*(3), 291–298.

Adams, D. R., & McFarland, L. Z. (1972). Morphology of the nasal fossae and associated structures of the hamster (Mesocricetus auratus). *Journal of Morphology*, *137*(2), 161–179.

Arencibia, A., Vazquez, J. M., Jaber, R., Gil, F., Ramirez, J. A., Rivero, M., Gonzalez, N., & Wisner, E. R. (2000). Magnetic Resonance Imaging and Cross Sectional Anatomy of the Normal Equine Sinuses and Nasal Passages. *Veterinary Radiology & Ultrasound*, *41*(4), 313–319.

Bide, R. W., Armour, S. J., & Yee, E. (2000). Allometric respiration/body mass data for animals to be used for estimates of inhalation toxicity to young adult humans. *Journal of Applied Toxicology*, *20*(4), 273–290.

Bojsen-Moller, F. (2004). Demonstration of Terminalis, Olfactory, Trigeminal and Perivascular Nerves in the Rat Nasal Septum. *The Journal of Comparative Neurology*, *159*(2), 245–256.

Bojsen-Moller, F., & Fahrenkrug, J. (1971). Nasal swell-bodies and cyclic changes in the air passage of the rat and rabbit nose. *Journal of Anatomy*, *110*(Pt 1), 25–37.

Callahan, J. R. (1993). Squirrels as predators. *Great Basin Naturalist*, *53*(2), 137–144.

Carleton, M. D., & Musser, G. G. (2005). *Mammal Species of the World* (3rd ed.). Johns Hopkins University Press.

Conchou, F., Sautet, J., Raharison, F., & Mogicato, G. (2012). Magnetic resonance imaging of normal nasal cavity and paranasal sinuses in cats. *Anatomia, Histologia, Embryologia*, *41*(1), 60–67.

Coppola, D., Craven, B., Seeger, J., & Weiler, E. (2014). The effects of naris occlusion on mouse nasal turbinate development. *The Journal of Experimental Biology*, *217*(12), 2044–2052.

Craven, B. A., Neuberger, T., Paterson, E. G., Webb, A. G., Josephson, E. M., Morrison, E. E., & Settles, G. S. (2007). Reconstruction and Morphometric Analysis of the Nasal Airway of the Dog (Canis familiaris) and Implications Regarding Olfactory Airflow. *The Anatomical Record*, *290*(11), 1325–1340.

Craven, B. A., Paterson, E. G., & Settles, G. S. (2010). The fluid dynamics of canine olfaction: unique nasal airflow patterns as an explanation of macrosmia. *Journal of the Royal Society, Interface / the Royal Society*, *7*(47), 933–943.

Deleon, V. B., & Smith, T. D. (2014). Mapping the Nasal Airways: Using Histology to Enhance CT-Based Three-Dimensional Reconstruction in Nycticebus. *The Anatomical Record*, *297*(11), 2113–2120.

Eiting, T. P., Smith, T. D., Perot, J. B., & Dumont, E. R. (2014). The role of the olfactory recess in olfactory airflow. *The Journal of Experimental Biology*, *217*(10), 1799–1803.

Evans, H. E. (1993). *Miller's Anatomy of the Dog* (3rd ed.). Philadelphia: W.B. Saunders Company.

Farke, A. A. (2010). Evolution and functional morphology of the frontal sinuses in Bovidae (Mammalia: Artiodactyla), and implications for the evolution of cranial pneumaticity. *Zoological Journal of the Linnean Society*, *159*(4), 988–1014.

Folkow, L. P., Blix, A. S., & Eide, T. J. (1988). Anatomical and functional aspects of the nasal mucosal and ophthalmic retia of phocid seals. *Journal of Zoology*, *216*(3), 417–436.

Green, P. A., Van Valkenburgh, B., Pang, B., Bird, D., Rowe, T., & Curtis, A. (2012). Respiratory and olfactory turbinal size in canid and arctoid carnivorans. *Journal of Anatomy*, *221*(6), 609–621.

Gross, E. A., Swenberg, J. A., Fields, S., & Popp, J. A. (1982). Comparative morphometry of the nasal cavity in rats and mice. *Journal of Anatomy*, *135*(Pt 1), 83–88.

Harkema, J. R., Carey, S. A., & Wagner, J. G. (2006). The nose revisited: a brief review of the comparative structure, function, and toxicologic pathology of the nasal epithelium. *Toxicologic Pathology*, *34*(3), 252–269.

Huntley, A. C., Costa, D. P., & Rubin, R. D. (1984). The contribution of nasal countercurrent heat exchange to water balance in the northern elephant seal, Mirounga angustirostris. *The Journal of Experimental Biology*, *113*, 447–454.

Jacob, A., & Chole, R. A. (2006). Survey anatomy of the paranasal sinuses in the normal mouse. *The Laryngoscope*, *116*(4), 558–563.

Kamau, J. M. Z., Maina, J. N., & Maloiy, G. M. O. (1984). The Design and the Role of the Nasal Passages in Temperature Regulation in the Dik-Dik Antilope (Rhynchotragus kirkii) with Observations on the Carotid Rete. *Respiration Physiology*, *56*(2), 183–194.

Kimbell, J. S., Godo, M. N., Gross, E. A., Joyner, D. R., Richardson, R. B., & Morgan, K. T. (1997). Computer Simulation of Inspiratory Airflow in All Regions of the F344 Rat Nasal Passages. *Toxicology and Applied Pharmacology*, *145*(2), 388–398.

Kumar, P., Kumar, S., & Singh, Y. (1993). Histological studies on the nasal ethmoturbinates of goats. *Small Ruminant Research*, *11*(1), 85–92.

Kumar, P., Timoney, J. F., Southgate, H. H. P., & Sheoran, A. S. (2000). Light and Scanning Electron Microscopic Studies of the Nasal Turbinates of the Horse. *Anatomia, Histologia, Embryologia*, *29*(2), 103–109.

Lawson, M. J., Craven, B. A., Paterson, E. G., & Settles, G. S. (2012). A computational study of odorant transport and deposition in the canine nasal cavity: Implications for olfaction. *Chemical Senses*, *37*(6), 553–566.

Lorensen, W. E., & Cline, H. E. (1987). Marching cubes: A high resolution 3D surface construction algorithm. *ACM SIGGRAPH Computer Graphics*, *21*(4), 163–169.

Loudon, C., & Tordesillas, A. (1998). The use of the dimensionless Womersley number to characterize the unsteady nature of internal flow. *Journal of Theoretical Biology*, *191*(1), 63–78.

Mery, S., Gross, E. A., Joyner, D. R., Godo, M., & Morgan, K. T. (1994). Nasal Diagrams: A Tool for Recording the Distribution of Nasal Lesions in Rats and Mice. *Toxicologic Pathology*, *22*(4), 353–372.

Moore, W. J. (1981). *The Mammalian Skull*. Cambridge: Cambridge University Press.

Negus, V. (1956). The air-conditioning mechanism of the nose. *British Medical Journal*, *1*(4963), 367–371.

Negus, V. (1958). *The Comparative Anatomy and Physiology of the Nose and Paranasal Sinuses*. London: E. & S. Livingstone Ltd.

Peacock, J., Jones, T., Tock, C., & Lutz, R. (1998). The onset of turbulence in physiological pulsatile flow in a straight tube. *Experiments in Fluids*, *24*(1), 1–9.

Ranslow, A. N., Richter, J. P., Neuberger, T., Van Valkenburgh, B., Rumple, C. R., Quigley, A. P., Pang, B., Krane, M. H., & Craven, B. A. (2014). Reconstruction and Morphometric Analysis of the Nasal Airway of the White-Tailed Deer (Odocoileus virginianus) and Implications Regarding Respiratory and Olfactory Airflow. *The Anatomical Record*, *297*(11), 2138–2147.

Reznik, G. K. (1990). Comparative Anatomy, Physiology, and Function of the Upper Respiratory Tract. *Environmental Health Perspectives*, *85*(4), 171–176.

Richter, J. P., Rumple, C. R., Neuberger, T., Pang, B., Van Valkenburgh, B., Ryan, T. M., Stecko, T. D., Yee, K. K., Wysocki, C. J., Krane, M. H., & Craven, B. A. (in preparation). Reconstruction and Morphometric Analysis of the Nasal Airway of the Eastern Grey Squirrel (Sciurus carolinensis) and Implications Regarding Respiratory and Olfactory Airflow.

Schmidt-Nielsen, K., Hainsworth, F. R., & Murrish, D. E. (1970). Counter-current heat exchange in the respiratory passages: effect on water and heat balance. *Respiration Physiology*, *9*(2), 263–276.

Schreider, J. P., & Hutchens, J. O. (1980). Morphology of the guinea pig respiratory tract. *The Anatomical Record*, *196*(3), 313–321.

Schreider, J. P., & Raabe, O. G. (1981). Anatomy of the Nasal-Pharyngeal Airway of Experimental Animals. *The Anatomical Record*, *200*(2), 195–205.

Schroeter, J. D., Kimbell, J. S., Asgharian, B., Tewksbury, E. W., & Singal, M. (2012). Computational fluid dynamics simulations of submicrometer and micrometer particle deposition in the nasal passages of a Sprague-Dawley rat. *Journal of Aerosol Science*, *43*(1), 31–44.

Stahl, W. R. (1967). Scaling of respiratory variables in mammals. *Journal of Applied Physiology*, *22*(3), 453–460.

Taubin, G. (1995). Curve and surface smoothing without shrinkage. In *Proceedings of the Fifth International Conference on Computer Vision, IEEE* (pp. 852–857).

Van Valkenburgh, B., Curtis, A., Samuels, J. X., Bird, D., Fulkerson, B., Meachen-Samuels, J., & Slater, G. J. (2011). Aquatic adaptations in the nose of carnivorans: evidence from the turbinates. *Journal of Anatomy*, *218*(3), 298–310.

Van Valkenburgh, B., Pang, B., Bird, D., Curtis, A., Yee, K., Wysocki, C., & Craven, B. A. (2014a). Respiratory and Olfactory Turbinals in Feliform and Caniform Carnivorans: The Influence of Snout Length. *The Anatomical Record*, *297*(11), 2065–2079.

Van Valkenburgh, B., Smith, T. D., & Craven, B. A. (2014b). Tour of a Labyrinth: Exploring the Vertebrate Nose. *The Anatomical Record*, *297*(11), 1975–1984.

Van Valkenburgh, B., Theodor, J., Friscia, A., Pollack, A., & Rowe, T. (2004). Respiratory turbinates of canids and felids: a quantitative comparison. *Journal of Zoology*, *264*(3), 281–293.

Wesson, D. W., Donahou, T. N., Johnson, M. O., & Wachowiak, M. (2008). Sniffing behavior of mice during performance in odor-guided tasks. *Chemical Senses*, *33*(7), 581–596.

Witmer, L. M., Sampson, S. D., & Solounias, N. (1999). The proboscis of tapirs (Mammalia: Perissodactyla): a case study in novel narial anatomy. *Journal of Zoology*, *249*(3), 249–267.

Youngentob, S. L., Mozell, M. M., Sheehe, P. R., & Hornung, D. E. (1987). A quantitative analysis of sniffing strategies in rats performing odor detection tasks. *Physiology & Behavior*, *41*(1), 59–69.

Academic Vita

Andrew Patrick Quigley
apq5001@psu.edu

EDUCATION

The Pennsylvania State University – The Schreyer Honors College — **University Park, PA**
College of Engineering, Integrated Undergraduate/Graduate (IUG) Program — *Class of 2015*

- Bachelor of Science in Bioengineering, Master of Science in Bioengineering
- Dean's List: 7 of 8 semesters

EXPERIENCE

Applied Research Laboratory — **University Park, PA**
Undergraduate/Graduate Researcher — *May 2012 to Present*

- Comparing anatomy and functional morphology of the mammalian nasal cavity.
- Reconstructing MRI/CT scans to yield 3D anatomical models of the nasal cavity of various mammals.
- Simulation development of airflow in nasal cavity based upon reconstructed 3D anatomical models.

Nanoscale Inorganic Solids Laboratory — **University Park, PA**
Undergraduate Researcher — *August 2011 to May 2012*

- Worked with a graduate student to create and observe chemical reactions under laboratory conditions.
- Created phase change molecules that are applicable to future technologies.
- Worked with products on the nanoscale.

QBC Diagnostics and The Drucker Company — **Port Matilda, PA**
Engineering Intern — *May 2011 to August 2011*

- Assisted with designs and redesigns of various models of centrifuges while assembling prototypes.
- Collaborated with Product Manager and Design Engineers on current projects for the company.
- Created solid model designs and drawings of centrifuge assemblies and centrifuge parts in SolidWorks.
- Worked on major project of internship by creating designs for a refrigerated centrifuge for the company.

PUBLICATIONS

Ranslow, A. N., Richter, J. P., Neuberger, T., Van Valkenburgh, B., Rumple, C. R., Quigley, A. P., Pang, B., Krane, M. H. and Craven, B. A. (2014). Reconstruction and Morphometric Analysis of the Nasal Airway of the White-Tailed Deer (*Odocoileus virginianus*) and Implications Regarding Respiratory and Olfactory Airflow. Anat Rec, 297: 2138–2147.

HONORS/AWARDS

Ram and Shanti Singh Scholarship — **Penn State University**
Awarded annually to a Schreyer Honors College Scholar — *Fall 2011 to Spring 2012*

The President's Freshman Award — **Penn State University**
Presented annually to freshman undergraduate degree candidates with a 4.00 GPA — *Spring 2011*

The Pre-eminence in Honors Education Fund — **Penn State University**
Awarded annually to a selected few Schreyer Honors College Scholars — *Fall 2010 to Spring 2011*

Eagle Scout, Troop 190, Boy Scouts of America — **Grantham, PA**
Renovated children's counseling room at Stop the Violence Ministry in Steelton, PA — *April 2010*

ACTIVITIES

Lion Ambassadors, The Penn State Student Alumni Corps — **Penn State University**
Executive Board, Alumni Status — *2012 to 2014*

Men's Water Polo Club Team — **Penn State University**
Vice President, THON Chair — *2010 to Present*

Biomedical Engineering Society — **Penn State University**
Member — *2010 to Present*